Pharyngeal mesoderm regulatory network controls cardiac and head muscle morphogenesis

Itamar Harel[1], Yoshiro Maezawa[2], Roi Avraham[1], Ariel Rinon[1], Hsiao-Yen Ma[3], Joe W. Cross[4], Noam Leviatan[5], Julius T. Hegesh[6], Achira Roy[7], Jasmine Jacob-Hirsch[8], Gideon Rechavi[8], Jaime Carvajal[4,9], Shubha Tole[7], Chrissa Kioussi[3], Sue Quaggin[2], and Eldad Tzahor[1]

1. Department of Biological Regulation, Weizmann Institute of Science, Rehovot, Israel.
2. Samuel Lunenfeld Research Institute, Toronto, Canada
3. Department of Pharmaceutical Sciences, College of Pharmacy, Oregon State University, Corvallis, OR, USA
4. Section of Gene Function and Regulation, The Institute of Cancer Research, London, UK
5. Department of Plant Sciences, Weizmann Institute of Science, Rehovot, Israel
6. Department of Pediatric Cardiology, Chaim Sheba Medical Center, Tel Aviv, Israel
7. Department of Biological Sciences, Tata Institute of Fundamental Research, Mumbai, India
8. Department of Pediatric Hemato-Oncology and Functional Genomics, Chaim Sheba Medical Center, Tel Aviv, Israel.
9. Centro Andaluz de Biología del Desarrollo, UPO-JA-CSIC, Seville, Spain.

*Corresponding author: Prof. Eldad Tzahor
Email: eldad.tzahor@weizmann.ac.il

Running title: Pharyngeal mesoderm regulatory network

Key words: Pharyngeal mesoderm, DiGeorge Syndrome, Lhx2, cardiogenesis, myogenesis

Summary

The search for developmental mechanisms driving vertebrate organogenesis has paved the way toward a deeper understanding of birth defects. During embryogenesis, parts of the heart and craniofacial muscles arise from pharyngeal mesoderm (PM) progenitors. Here, we reveal a hierarchical regulatory network of a set of transcription factors expressed in the PM that initiates heart and craniofacial organogenesis. Genetic perturbation of this network in mice resulted in heart and craniofacial muscle defects, revealing robust cross-regulation between its members. We identified Lhx2 as a novel player during cardiac and pharyngeal muscle development. Lhx2 and Tcf21 genetically interact with Tbx1, the major determinant in the etiology of DiGeorge/velo-cardio-facial/22q11.2 deletion syndrome. Furthermore, knockout of these genes in the mouse recapitulates specific cardiac features of this syndrome. We suggest that PM-derived cardiogenesis and myogenesis are network properties rather than properties specific to individual PM members. These findings shed new light on the developmental underpinnings of congenital defects.

\body

Introduction

Embryonic development encompasses an orchestrated series of cellular events; even subtle alterations in this process can lead to serious disorders. Gene regulatory networks are thought to play key roles during organogenesis. Such developmental networks have been identified in *Echinoidea* (sea urchin), *Drosophila, Ciona intestinalis* and *C. elegans* (1); the characterization of gene regulatory networks during vertebrate organogenesis lags behind.

Pharyngeal mesoderm (PM) cells are a subset of the head mesoderm, contributing to broad regions of the heart and head musculature. The PM contains initially both paraxial and splanchnic mesoderm cells surrounding the pharynx. Later, these cells migrate to fill the core of the pharyngeal arches, also known as branchial arches (2). Prior to their differentiation, PM cells express both skeletal muscle and second heart field markers. Thus, the genetic program controlling early pharyngeal muscle development overlaps with that of the heart; the major molecular players include the transcription factors Tbx1, Pitx2, Tcf21 (capsulin/Pod1), Islet1 and Msc (MyoR) (2-5).

In addition to pharyngeal muscles, PM cells also contribute to the arterial pole of the heart, following the formation of the linear heart tube. Perturbations in the recruitment of PM-derived cells to the heart tube can lead to a wide range of congenital heart defects. Such defects occur in nearly 1% of live births, reflecting the complex cellular processes underlying heart development (6-8). Cardiac and craniofacial birth defects are often linked, due to their anatomical proximity during early embryogenesis and overlapping progenitor populations (2-4). One such congenital defect is DiGeorge syndrome (DGS), the most frequent microdeletion syndrome in humans, with an estimated incidence of 1 in 4,000 live births (9, 10). Its clinical features vary, and may include cardiac defects, craniofacial and aortic arch anomalies, as well as thymus and parathyroid gland hypoplasia.

The T-box transcription factor 1 (TBX1) is located in the 22q11.2 deleted region, and mutations in TBX1 have been found in some patients with DGS-like phenotype; therefore, TBX1 haploinsufficiency is probably a major contributor to human del22q11 phenotypes, and to murine models of the syndrome (11-14).

How does a set of PM transcription factors execute myogenesis and cardiogenesis? What are the relationships between these factors? Could we identify new PM regulators? In this study we have addressed these questions in mice by revealing a hierarchical regulatory network, composed of a set of transcription factors expressed in PM progenitors. A comprehensive genetic study uncovered novel molecular evidence for the involvement of the PM regulatory network in myogenesis and cardiogenesis as well as in the etiology of DGS.

Results

In order to identify novel regulators of PM myogenic progenitors, we compared gene expression patterns of PM-derived progenitors, to those derived from the trunk (somites) at early stages of embryonic development in the mouse (E9.5-E11.5). Myf5 is the earliest marker of myogenic commitment (15). In *Myf5*^{Cre};*Rosa26*^{YFP} double heterozygous embryos the entire skeletal muscle lineage is YFP^{+} (Fig. 1A'). We FACS-purified PM and trunk myogenic progenitors separately, and evaluated their gene expression profiles using an Affimetrix array (Fig. 1A-D). Our results confirmed the differential expression of previously described PM-specific transcription factors such as *Tcf21, Isl1*, *Tbx1, Msc, Pitx2,* and *Nkx2.5* (Figs. 1E and S1). Other markers, such as *Tlx1* (16), *Six2* (17)*,* the endothelial marker *Lmo2* (18), the endothelin signaling component *Edn1* (19), and retinoic acid-related genes were identified in our screen, and were enriched in PM, compared to the trunk progenitors (Figs. 1E and S1). As expected, *Pax3*, the key myogenic regulator of trunk skeletal muscles, was not expressed in PM progenitors. Consistent with the fact that myogenic differentiation in head muscle progenitors lags behind that of the trunk, we observed delayed activation of muscle contractile genes such as myosins (e.g. *Myh3*) and troponins (e.g. *Tnni1*) in the PM, relative to trunk muscle progenitors (Fig. 1E). In addition, we identified *Lhx2*, a LIM

domain-containing transcription factor, as a novel PM-specific gene. *In situ* hybridization revealed that *Lhx2* is expressed in the mesodermal core of the pharyngeal arches (Fig. 1F-I), while completely absent from the somites. In mice, Lhx2 is a prerequisite for the development of several organs, including the eye, telencephalon, and blood system (20-22), which fits its expression in these tissues (Fig. 1F-I).

In order to obtain detailed expression relationships of Lhx2 relative to other lineages within the pharyngeal arches we immunostained control E9.5 embryos with antibodies to Lhx2, Isl1, AP2 and Pecam1 (Figs. 1J-L and S2). Most cells in the core of the arch express both Lhx2 and Isl1. In contrast, Lhx2 is not expressed in neural crest (AP2) or endothelial (Pecam1) cells (Figs. 1J-L and S2). Isl1 is expressed in, and required for a broad subset of cardiac progenitors in the mouse (23, 24). Isl1 is expressed in the distal part of the PM and these cells contribute to both pharyngeal muscles (and their satellite cells) as well as to the heart (2). A stream of $Lhx2^{+}$ $Isl1^{+}$ PM cells can be seen connecting the second pharyngeal arch and the outflow tract (OFT). Taken together, the expression pattern of Lhx2 in $Isl1^{+}$ PM progenitors suggests that this gene might play a role in both myogenesis and cardiogenesis processes.

Next we determined the genetic interactions between the major PM factors at E9.5 (Fig. 2). To systematically examine the epistatic relationships between the major PM regulators, we used several mouse knockout models (Figs. 2 and S3). While *Tbx1* and *Tcf21* expression patterns remained unchanged in *Lhx2* mutant embryos (Fig. 2A-B'), *Lhx2* expression was reduced in the PM of *Tbx1* mutant embryos at the same developmental stage (Fig. 2C,C'). These results suggest that Lhx2 acts downstream of Tbx1. The expression levels of *Tcf21*, *Msc* and *Pitx2*, were slightly increased in the PM of *Tbx1* mutant embryos, consistent with findings from a recent screen for Tbx1 target genes (25) (Figs. 2D,D' and S3), suggesting that these factors are regulated by Tbx1.

Next we examined how the bHLH factor Tcf21 affects the PM regulators. It was previously shown that a subgroup of pharyngeal muscles was absent in *Tcf21*/*Msc* double knockout embryos (26).

Furthermore, these two genes have been shown to regulate the expression of *MyoD* and *Myf5* in craniofacial muscle progenitors (27). The expression of *Lhx2*, *Tbx1* and *Pitx2* was reduced in the PM of *Tcf21* mutant embryos (Figs. 2E-F' and S3). These findings place Tcf21 in the upper tier of the PM genetic network.

Finally we have characterized the bicoid-related homeodomain transcription factor Pitx2. Both pharyngeal muscles (derived from the first arch) and extraocular muscles (EOM) were affected in *Pitx2* knockout embryos (17, 28). Pitx2 and Tbx1 were shown to be genetically linked in many developmental processes, including cardiac and craniofacial muscle development (3). In *Pitx2* knockout embryos, *Tbx1* was hardly detected in the PM, and *Lhx2* was diminished specifically in the mesoderm of the first pharyngeal arch (Fig. S3). We confirmed the observed changes in gene expression using qRT-PCR on isolated pharyngeal arches (1^{st}-3^{rd}) of various mutant embryos (Fig. S4). The results are consistent with the gene expression patterns observed by *in situ* hybridization (Figs. 2 and S3). Notably, some of the analyzed genes (e.g., *Pitx2* and *Tbx1*) are also expressed in the ectoderm and endoderm of the pharyngeal arches; accordingly their total levels were moderately changed compared to the *in situ* hybridization results (Fig. S4). Notably, despite some loss of PM cells in *Pitx2* mutants at E9.5, which underscores the importance of Pitx2 in PM cell survival (17, 28), the observed changes in gene expression patterns could not be attributed to loss of PM cells (Fig. S4B). Our findings reveal cross-regulation between members of the PM network: Tcf21 and Pitx2 are linked to Tbx1, while Lhx2 lies downstream to these genes.

A key question regarding our findings is whether the observed changes in PM gene expression (Figs. 2A-F' and S3) are due to direct interactions between the PM transcription factors. Chromatin immunoprecipitation (ChIP) was performed on isolated E9.5 pharyngeal arch tissues using Tbx1, Pitx2 and Tcf21 antibodies in order to evaluate a potential cross regulation between PM members. Our results suggest several interactions, the strongest of which are Tbx1, Pitx2 and Tcf21 with *Pitx2* proximal promoter (Fig. 2G). Due to the extensive interactions of Pitx2 with other PM members, we decided to further characterize its specific binding sites using ChIP-seq. Pitx2 binding to *Tbx1, Tcf21* and *Lhx2* regulatory regions was enriched in isolated E9.5 pharyngeal arch

tissues (Fig. 2H). As a control, we compared the binding of Pitx2 to these elements in *Pitx2*$^{-/-}$ derived tissues, binding of Pitx2 to non-specific genomic sites, as well as binding of non-specific antibody (Figs. 2H and S5). Although Pitx2 did not bind to the *Tbx1* proximal promoter, we could identify its binding to specific sites upstream to the promoter using a ChIP-seq approach (Figs. 2H and S5). Taken together, our findings suggest that the PM regulatory network involves extensive genetic interactions between its members (Fig. 2I).

The involvement of Lhx2 in cardiac and craniofacial development was not previously examined, partly due to the fact that *Lhx2* knockout mouse embryos die at E15.5 (20). Therefore, we first sought to address its role during head muscle development (Fig. 3). Pax7 marks muscle progenitors whereas MyoD defines a more committed myogenic state. At E11.5, the total number of myogenic cells (Pax7^{+} or MyoD^{+}) in the PM of *Lhx2* mutant embryos decreased by approximately 50% (Fig. 3A-F). Comparing the ratio between MyoD and Pax7 expressing cells in control *vs*. *Lhx2* mutants revealed that the Pax7^{+} population was more affected, suggesting that Lhx2 is required in PM-derived muscle progenitors.

A decrease in the number of muscle progenitors could be due to either a delay in the specification of PM cells toward the myogenic lineage, a decrease in their proliferation, or elevated apoptosis. To resolve this issue, we compared myogenic (Pax7^{+}-MyoD^{+}) *vs*. pre-myogenic PM progenitors expressing Isl1^{+}. Isl1 expression is downregulated rapidly as head myogenesis ensues, and Isl1 overexpression in chick embryos delayed myogenic differentiation (29, 30). In *Lhx2* mutants, Isl1 expression failed to be downregulated in the core of the 1st pharyngeal arch compared to controls (Fig. 3G-I), while cell proliferation and apoptosis remained comparable (Figs. 3J-L and S6). The observed increase in pre-myogenic Isl1^{+} cells in *Lhx2* mutants was inversely correlated with the number of Pax7 expressing cells, suggesting that Lhx2 is involved in pharyngeal muscle specification.

Myf5 is highly regulated, both spatially and temporally by various factors (31). In order to further examine the role of Lhx2 during head muscle specification, we utilized the *Myf5*^{nLacZ} reporter (32).

Myf5 expression in the pharyngeal arches was reduced in *Lhx2* mutant compared to control E11.5 embryos, while trunk and extraocular muscles (EOM) remained unaffected (Fig. 3M,N; n≥12). These findings demonstrate that Lhx2 is required for the early activation of *Myf5* in the myogenic specification program within the pharyngeal arches. The expression of *Myf5* (LacZ staining) was largely restored at E14.5, albeit with some patterning defects (Fig. 3O,P). Hence, the PM regulatory network acts to provide robustness by allowing the activation of the myogenic program in the absence of a single PM member, consistent with previous studies (16, 33).

Next, we examined whether *Myf5* is directly regulated by the members of the PM network by *in-vivo* ChIP. Tbx1, Pitx2 and Tcf21 were associated to the *Myf5* evolutionary conserved region (ECR-84), which is part of the mandibular arch enhancer (MAE, Fig. S5) (31). To further explore the connection between Lhx2 and *Myf5*, we identified three putative Lhx2 binding sites within the *Myf5* MAE. Next, C2C12 cells, transfected with *Lhx2-HA* construct were used for a ChIP experiment using anti-HA antibody. We found that Lhx2 can bind to one of these sites in C2C12 cells (Fig. S5).

To further validate the robust nature of the myogenic program in the head we compared single knockouts of PM factors (Fig. 4A-D). Knockout of *Lhx2*, *Tbx1* and *Tcf21* separately, revealed muscle patterning defects in all three mutants (Fig. 4A-D). In agreement with an earlier report (16), pharyngeal muscles are severely perturbed, though not completely eliminated, in $Tbx1^{-/-}$ mutants [(Fig. 4C and (16, 33)]. In order to investigate the genetic wiring of the PM regulators, we analyzed the muscle phenotype in double knockout embryos (Fig. 4E-I). The muscle phenotype in $Tbx1^{-/-}$ mutants was comparable to that of $Tbx1^{-/-};Lhx2^{-/+}$ mutants (Fig. 4C,E). Remarkably, pharyngeal arch muscles were completely missing in $Tbx1^{-/-};Lhx2^{-/-}$ double mutants (Fig. 4F; n=2/4). Likewise, pharyngeal muscles were eliminated in most $Tbx1^{-/-};Myf5^{-/-}$ mutants (Fig. 4G; n=3/4), in agreement with (33).

Taken together, our findings reveal that Tbx1, Lhx2, Myf5 genetic circuit is required for pharyngeal muscle specification. Our findings suggest that in the absence of both Myf5 and Lhx2, Tbx1, could

initiate myogenesis by activating *MyoD* via a parallel genetic pathway, as suggested by (33). Accordingly, pharyngeal muscles of *Tbx1*$^{-/-}$;*MyoD*$^{-/-}$ double mutants were completely missing (with the exception of the digastric muscles in the lower jaw) (Fig. 4I; n=2/2). Hence, in the absence of Tbx1 and another factor (e.g., Lhx2, Myf5, or MyoD) pharyngeal muscles are severely perturbed. Consistent with the key role of Tbx1 in this genetic network, *Myf5*$^{-/-}$;*Lhx2*$^{-/-}$ and *MyoD*$^{-/-}$;*Lhx2*$^{-/-}$ double-knockout embryos did not show an enhanced muscle phenotype, compared to each knockout alone (Figs. 4H and S4). Our findings suggest that the PM network acts to ensure proper myogenesis in the absence of single PM members (Fig. 4J).

DGS is a common congenital disease involving cardiac and craniofacial defects. The major genetic determinant in its etiology is TBX1, although other genes in the 22q11 region have been shown to be involved. Because *Lhx2* lies downstream of Tbx1 We hypothesized that *Lhx2* mutant embryos might display DGS phenotypes. *Lhx2* mutants die at E14.5-15.5 from severe anemia and developmental defects (20). The development of the ventricular septum, is completed at E15, thus we analyzed both standard and conditional Lhx2 null embryos around this stage. *Lhx2* was ablated in the cardio-craniofacial mesoderm using the *MesP1*^{Cre} mouse line (34), which prolongs their viability up to birth. Indeed, at E17.5, about 50% of *MesP1*$^{Cre+/-}$;*Lhx2*$^{-/floxed}$ (*Lhx2*^{mKO}) mutants exhibited DGS-like cardiac defects, including various outflow-tract anomalies such as ventricular septal defect (VSD), tetralogy of Fallot (TOF), and double outlet right ventricle (DORV) (Fig. 5; n=7/13; and Supplementary Table 1). Interestingly, aortic arch patterning, one of the most common features of DGS, was normal in all *Lhx2*^{mKO} mutants (n=13/13; and in E14.5 *Lhx2*$^{-/-}$ embryos n=10/10; Fig. 5A-E and Supplementary Table 1).

We next investigated the genetic interaction between Tbx1 and Lhx2, by measuring the frequency of VSD in compound mutants. While *Tbx1*$^{+/-}$ heterozygous embryos had no detectable VSD (n=11), 20% of *Tbx1*$^{+/-}$*Lhx2*$^{+/-}$ double heterozygous (compound) embryos had VSD (n=10) (Supplementary Table 1). This functional interaction strongly suggests that Tbx1 and Lhx2 are in the same genetic pathway and synergistically regulate heart morphogenesis.

In order to identify genes lying downstream of Lhx2, we examined the expression of several possible candidates. The expression levels of both *Fgf8*, which is genetically linked to Tbx1 in the context of DGS (35), and *Bmp4*, which was shown to act downstream of Lhx2 during eye development (36), were comparable in *Lhx2* mutant and control embryos (Fig. S7A-D). Several recent studies have shown that both cardiac neural crest (affecting caudal PM progenitors) and cranial neural crest cells (affecting rostral/cranial PM progenitors) influence the migration of PM cells into the looping heart, and their subsequent differentiation (2, 37). We therefore examined the expression pattern of several neural crest markers, *Dlx5, Twist* and *Sox10* as well as the PM marker, *Isl1*. Although *Isl1*, *Dlx5* and *Twist* expression seemed to be comparable in *Lhx2* mutants and controls, *Sox10* expression pattern was slightly perturbed in some mutants, suggesting that neural crest cell migration might play some role in the observed phenotype (Fig. S7E-J). These findings suggest that perturbation of the PM regulatory network affects cardiac formation both cell autonomously and non-cell autonomously, via crosstalk with neural crest cells.

Given the regulatory interactions between various network members, we hypothesized that elimination of each of the core factors, one-by-one, might elicit a DGS-like phenotype either directly, or by affecting Tbx1 levels. Consistent with this view, Pitx2 is known to affect cardiac development (38, 39). Because *Tbx1* levels were reduced in *Tcf21* mutants (Fig. 2) we sought to better analyze the heart phenotype of these mutants. *Tcf21* mutants display TOF, including VSD, overriding aorta, pulmonic stenosis (Figs. 5N-R, S8 and Supplementary Table 1) as well as cleft palates (Fig. 4D). Similar to $Lhx2^{mKO}$ mutant embryos, the morphology of the aortic arch remained normal in *Tcf21* mutants. Furthermore, hearts of $Tcf21^{-/-}$ mutants displayed regions of epicardial detachments (Fig. S8) in agreement with a recent report (40). Taken together, insights from the PM network composition, led us to predict that both Tcf21 and Lhx2, which are genetically linked to Tbx1, might cause cardiac defects. We demonstrate such cardiac anomalies in both *Tcf21* and *Lhx2* mutant embryos, some of which are shared by DGS patients.

Discussion

Our results demonstrate that a set of transcription factors expressed in PM progenitors form a regulatory network that coordinates normal heart and craniofacial development (Fig. 6A). The expression of PM members (*Tbx1, Pitx2, Tcf21,* and *Lhx2*) is regulated by other members of the network, and involves direct genetic interactions. Lhx2 is a novel player within the PM network; knockout of this gene resulted in a pharyngeal muscle specification defect, as well as DGS-like phenotypes (Fig. 6A). We revealed epistatic relationships between Tbx1, Lhx2, and Myf5 embedded within the PM network, affecting early pharyngeal muscle specification and patterning. Thus, Lhx2 plays an important role in PM progenitor cells, consistent with its roles in the specification of other stem/progenitor cell populations such as telencephalic progenitors (41); retina progenitors (42); hematopoietic progenitors (43); and hair follicle progenitors (21).

In addition, we revealed a genetic link between *Tcf21, Tbx1,* and *Lhx2* in the PM transcriptional circuit. Genetic perturbation of these factors resulted in specific DGS-like phenotypes. We demonstrated using single and double knockout experiments that Lhx2 removal has specific cardiac phenotypes, and it enhances the severity of both craniofacial muscles and heart phenotypes of *Tbx1* mutants. This suggests that both genes work in the same genetic pathway. Hence, Lhx2 can be included within the growing list of transcription factors that have been found to play important roles in second heart field development, based on the cardiac phenotypes of single and compound mutations in these genes (44).

Although human *TCF21* and *LHX2* do not map to chromosome 22q11.2, the shared morphological defects and link to Tbx1 suggest that these genes might be genetic modifiers of DGS. Genetic variations in the *ISL1* locus in human were shown to be linked to an increased risk for congenital heart defects (45). Could *LHX2* and *TCF21* contribute to the variations in cardiovascular phenotype seen in DGS patients? To draw genotype-phenotype correlations in such patients, a genome-wide association study, as well as a candidate gene approach, is currently underway. Results from this study could shed light on whether common DNA variants alter the degree of expressivity of the syndrome.

One of the enigmatic features of DGS is that it varies in its penetrance from patient to patient. Importantly, some DGS patients do not display neither a deletion nor a mutation in the *Tbx1* locus (46). Changes in the levels of Tbx1, loss and gain, lead to a dose-dependent spectrum of DGS malformations (47, 48). Therefore, Tbx1 levels must be precisely regulated, in order for the pharyngeal apparatus and its derivatives to properly form. Our study adds to the understanding of how Tbx1 levels could be fine-tuned by interactions with other PM transcription factors (Fig. 6A).

Tbx1 is expressed in both rostral and caudal PM cells. It has been shown that cranial PM cells enter the arterial pole of the heart to populate the RV and OFT, while caudal PM cells contribute to the myocardium at the base of the great arteries (49). Previous studies addressing DGS etiology reported various cardiac anomalies, including both aortic arch and cardiac defects, for the following knockout models: *Fgf8* and *Six1/Eya1* (35), *VegfA* (50) and retinoic acid-related genes (51). We suggest that Lhx2 and Tcf21, expressed in the cranial PM, function as domain-specific modifiers of the *Tbx1* pathway, as judged by the uncoupling of the aortic arch phenotype from that of the outflow tract (Fig. 6B). In sum, our study sheds light on the developmental principles underlying the etiology of congenital birth defects.

Our findings imply that the heart and pharyngeal muscles show varying degrees of sensitivity to early perturbations of the PM. For example, while the pharyngeal muscle phenotypes of *Lhx2* and *Tcf21* mutants are largely restored, albeit with patterning/hypoplastic defects, the cardiac defects are beyond repair. Detailed analyses of pharyngeal muscles in mouse and zebrafish DGS models (or in human patients) have not been well-characterized. Facial asymmetry, for example, is a rare symptom observed in babies only when they cry, known as “asymmetric crying faces,” is caused by the absence or hypoplasia of a pharyngeal muscle at the corner of the mouth. This defect has been shown to be associated with cardiovascular anomalies in DGS babies (52). Therefore, it would be important to better characterize the linkage between craniofacial muscle patterning and cardiovascular defects.

Regulatory networks of transcription factors have been found in diverse organisms, from bacteria to humans. The network architectures of the transcription factors function to enhance the stability of gene expression and functional outputs. The PM network characteristics that we (this study) and others (16, 17, 28, 33) have gradually uncovered in recent years seem to be hierarchical, and involve extensive cis-regulatory interactions. We propose that the overall biological outputs of the PM network (e.g., cardiogenesis and myogenesis) and precise signal strengths are network properties, rather than properties specific to individual PM members.

Experimental Procedures

Mice

The following mouse transgenic lines and their genotyping have been previously described: *Myf5*^{Cre} (53), Rosa26^{YFP} (54), *Pitx2*$^{-/-}$ (55), *Myf5*^{nlacZ} (32), *MesP1*^{Cre} (34), *Lhx2*^{sKO} (20), *Lhx2*^{cKO} (22), *Tcf21*$^{-/-}$ (56) and *Tbx1*$^{-/-}$ (11).

FACS, Microarrays, Staining, qPCR and ChIP

Inter-limb somites and pharyngeal arches were dissected from E9.5, E10.5 and E11.5 *Myf5*^{Cre}*;Rosa*^{YFP} mouse embryos. RNA was purified amplified, and hybridized to Affymetrix arrays (detailed in the Supplementary Information). X-Gal staining, histology, immunohistochemistry and whole-mount in situ hybridization were performed as previously reported (29). Antibodies are listed in the Supplementary Information. cDNA or immunoprecipitated (IP) DNA was analyzed by qPCR using SYBR Green methodology as recommended by the manufacturer. Primers used are listed in supplemental Table 2. The ChIP was done according to (57). Minor modifications and antibodies used are detailed in the Supplementary Information.

Acknowledgments

This work was supported by grants to E.T. from the European Research Council; Israel Science Foundation; United States-Israel Binational Science Foundation; German Israeli Foundation; Association Française Contre les Myopathies; Kirk Center for Childhood Cancer and

Immunological Disorders; Jeanne and Joseph Nissim Foundation for Life Sciences Research; and a donation from the Jack Gitlitz Estate. CK was supported by NIH-NIAMS grant AR054406. J.W.C was supported by a Studentship from The Institute Of Cancer Research, London. J.J.C. was partly supported by a Ministry of Science and Innovation (MICINN) grant [BFU2011-22928]. We thank Kfir-Baruch Umansky for his technical help and advice, and Karina Yaniv, Bernice Morrow and Robert Kelly for insightful discussions.

References:

1. Davidson EH (2010) Emerging properties of animal gene regulatory networks. *Nature* 468(7326):911-920.
2. Tzahor E & Evans SM (2011) Pharyngeal mesoderm development during embryogenesis: implications for both heart and head myogenesis. *Cardiovasc Res*:196-202.
3. Grifone R & Kelly RG (2007) Heartening news for head muscle development. *Trends Genet* 23(8):365-369.
4. Tzahor E (2009) Heart and craniofacial muscle development: a new developmental theme of distinct myogenic fields. *Dev Biol* 327(2):273-279.
5. Sambasivan R, Kuratani S, & Tajbakhsh S (2011) An eye on the head: the development and evolution of craniofacial muscles. *Development* 138(12):2401-2415.
6. Buckingham M, Meilhac S, & Zaffran S (2005) Building the mammalian heart from two sources of myocardial cells. *Nat Rev Genet* 6(11):826-835.
7. Hutson MR & Kirby ML (2003) Neural crest and cardiovascular development: a 20-year perspective. *Birth Defects Res C Embryo Today* 69(1):2-13.
8. Srivastava D (1999) Developmental and genetic aspects of congenital heart disease. *Curr Opin Cardiol* 14(3):263-268.
9. Baldini A (2005) Dissecting contiguous gene defects: TBX1. *Curr Opin Genet Dev* 15(3):279-284.
10. Yamagishi H & Srivastava D (2003) Unraveling the genetic and developmental mysteries of 22q11 deletion syndrome. *Trends Mol Med* 9(9):383-389.
11. Lindsay EA*, et al.* (2001) Tbx1 haploinsufficieny in the DiGeorge syndrome region causes aortic arch defects in mice. *Nature* 410(6824):97-101.
12. Yagi H*, et al.* (2003) Role of TBX1 in human del22q11.2 syndrome. *Lancet* 362(9393):1366-1373.
13. Jerome LA & Papaioannou VE (2001) DiGeorge syndrome phenotype in mice mutant for the T-box gene, Tbx1. *Nat Genet* 27(3):286-291.
14. Merscher S*, et al.* (2001) TBX1 is responsible for cardiovascular defects in velo-cardio-facial/DiGeorge syndrome. *Cell* 104(4):619-629.
15. Sambasivan R & Tajbakhsh S (2007) Skeletal muscle stem cell birth and properties. *Semin Cell Dev Biol* 18(6):870-882.
16. Kelly RG, Jerome-Majewska LA, & Papaioannou VE (2004) The del22q11.2 candidate gene Tbx1 regulates branchiomeric myogenesis. *Hum Mol Genet* 13(22):2829-2840.
17. Shih HP, Gross MK, & Kioussi C (2007) Cranial muscle defects of Pitx2 mutants result from specification defects in the first branchial arch. *Proc Natl Acad Sci U S A* 104(14):5907-5912.
18. Landry JR*, et al.* (2005) Fli1, Elf1, and Ets1 regulate the proximal promoter of the LMO2 gene in endothelial cells. *Blood* 106(8):2680-2687.
19. Thomas T*, et al.* (1998) A signaling cascade involving endothelin-1, dHAND and msx1 regulates development of neural-crest-derived branchial arch mesenchyme. *Development* 125(16):3005-3014.
20. Porter FD*, et al.* (1997) Lhx2, a LIM homeobox gene, is required for eye, forebrain, and definitive erythrocyte development. *Development* 124(15):2935-2944.
21. Rhee H, Polak L, & Fuchs E (2006) Lhx2 maintains stem cell character in hair follicles. *Science* 312(5782):1946-1949.
22. Mangale VS*, et al.* (2008) Lhx2 selector activity specifies cortical identity and suppresses hippocampal organizer fate. *Science* 319(5861):304-309.
23. Cai CL*, et al.* (2003) Isl1 identifies a cardiac progenitor population that proliferates prior to differentiation and contributes a majority of cells to the heart. *Dev Cell* 5(6):877-889.
24. Laugwitz KL, Moretti A, Caron L, Nakano A, & Chien KR (2008) Islet1 cardiovascular progenitors: a single source for heart lineages? *Development* 135(2):193-205.
25. Liao J*, et al.* (2008) Identification of downstream genetic pathways of Tbx1 in the second heart field. *Dev Biol* 316(2):524-537.
26. Lu JR*, et al.* (2002) Control of facial muscle development by MyoR and capsulin. *Science* 298(5602):2378-2381.

27. Moncaut N*, et al.* (2012) Musculin and TCF21 coordinate the maintenance of myogenic regulatory factor expression levels during mouse craniofacial development. *Development* 139(5):958-967.
28. Dong F*, et al.* (2006) Pitx2 promotes development of splanchnic mesoderm-derived branchiomeric muscle. *Development* 133(24):4891-4899.
29. Harel I*, et al.* (2009) Distinct origins and genetic programs of head muscle satellite cells. *Dev Cell* 16(6):822-832.
30. Nathan E*, et al.* (2008) The contribution of Islet1-expressing splanchnic mesoderm cells to distinct branchiomeric muscles reveals significant heterogeneity in head muscle development. *Development* 135(4):647-657.
31. Carvajal JJ, Cox D, Summerbell D, & Rigby PW (2001) A BAC transgenic analysis of the Mrf4/Myf5 locus reveals interdigitated elements that control activation and maintenance of gene expression during muscle development. *Development* 128(10):1857-1868.
32. Tajbakhsh S, Rocancourt D, & Buckingham M (1996) Muscle progenitor cells failing to respond to positional cues adopt non-myogenic fates in myf-5 null mice. *Nature* 384(6606):266-270.
33. Sambasivan R*, et al.* (2009) Distinct regulatory cascades govern extraocular and pharyngeal arch muscle progenitor cell fates. *Dev Cell* 16(6):810-821.
34. Saga Y*, et al.* (1999) MesP1 is expressed in the heart precursor cells and required for the formation of a single heart tube. *Development* 126(15):3437-3447.
35. Guo C*, et al.* (2011) A Tbx1-Six1/Eya1-Fgf8 genetic pathway controls mammalian cardiovascular and craniofacial morphogenesis. *J Clin Invest* 121(4):1585-1595.
36. Yun S*, et al.* (2009) Lhx2 links the intrinsic and extrinsic factors that control optic cup formation. *Development* 136(23):3895-3906.
37. Rochais F, Mesbah K, & Kelly RG (2009) Signaling pathways controlling second heart field development. *Circ Res* 104(8):933-942.
38. Nowotschin S*, et al.* (2006) Tbx1 affects asymmetric cardiac morphogenesis by regulating Pitx2 in the secondary heart field. *Development* 133(8):1565-1573.
39. Ai D*, et al.* (2006) Pitx2 regulates cardiac left-right asymmetry by patterning second cardiac lineage-derived myocardium. *Dev Biol* 296(2):437-449.
40. Acharya A*, et al.* (2012) The bHLH transcription factor Tcf21 is required for lineage-specific EMT of cardiac fibroblast progenitors. *Development* 139(12):2139-2149.
41. Chou SJ, Perez-Garcia CG, Kroll TT, & O'Leary DD (2009) Lhx2 specifies regional fate in Emx1 lineage of telencephalic progenitors generating cerebral cortex. *Nat Neurosci* 12(11):1381-1389.
42. Tetreault N, Champagne MP, & Bernier G (2009) The LIM homeobox transcription factor Lhx2 is required to specify the retina field and synergistically cooperates with Pax6 for Six6 trans-activation. *Dev Biol* 327(2):541-550.
43. Dahl L, Richter K, Hagglund AC, & Carlsson L (2008) Lhx2 expression promotes self-renewal of a distinct multipotential hematopoietic progenitor cell in embryonic stem cell-derived embryoid bodies. *PLoS ONE* 3(4):e2025.
44. Kelly RG (2012) The second heart field. *Curr Top Dev Biol* 100:33-65.
45. Stevens KN*, et al.* (2010) Common variation in ISL1 confers genetic susceptibility for human congenital heart disease. *PLoS ONE* 5(5):e10855.
46. Scambler PJ (2010) 22q11 deletion syndrome: a role for TBX1 in pharyngeal and cardiovascular development. *Pediatr Cardiol* 31(3):378-390.
47. Zhang Z & Baldini A (2008) In vivo response to high-resolution variation of Tbx1 mRNA dosage. (Translated from eng) *Hum Mol Genet* 17(1):150-157 (in eng).
48. Liao J*, et al.* (2004) Full spectrum of malformations in velo-cardio-facial syndrome/DiGeorge syndrome mouse models by altering Tbx1 dosage. *Hum Mol Genet* 13(15):1577-1585.
49. Lescroart F*, et al.* (2010) Clonal analysis reveals common lineage relationships between head muscles and second heart field derivatives in the mouse embryo. *Development* 137(19):3269-3279.
50. Stalmans I*, et al.* (2003) VEGF: a modifier of the del22q11 (DiGeorge) syndrome? *Nat Med* 9(2):173-182.

51. Roberts C, Ivins S, Cook AC, Baldini A, & Scambler PJ (2006) Cyp26 genes a1, b1 and c1 are down-regulated in Tbx1 null mice and inhibition of Cyp26 enzyme function produces a phenocopy of DiGeorge Syndrome in the chick. *Hum Mol Genet* 15(23):3394-3410.
52. Stewart HS & Clayton-Smith J (1996) 22q11 deletion: a cause of asymmetric crying facies. *Arch Dis Child* 75(1):89.
53. Tallquist MD, Weismann KE, Hellstrom M, & Soriano P (2000) Early myotome specification regulates PDGFA expression and axial skeleton development. *Development* 127(23):5059-5070.
54. Srinivas S*, et al.* (2001) Cre reporter strains produced by targeted insertion of EYFP and ECFP into the ROSA26 locus. *BMC Dev Biol* 1:4.
55. Lin CR*, et al.* (1999) Pitx2 regulates lung asymmetry, cardiac positioning and pituitary and tooth morphogenesis. *Nature* 401(6750):279-282.
56. Quaggin SE*, et al.* (1999) The basic-helix-loop-helix protein pod1 is critically important for kidney and lung organogenesis. *Development* 126(24):5771-5783.
57. Hilton T, Gross MK, & Kioussi C (2010) Pitx2-dependent occupancy by histone deacetylases is associated with T-box gene regulation in mammalian abdominal tissue. *J Biol Chem* 285(15):11129-11142.

Figure 1: Lhx2, a novel pharyngeal mesoderm regulator

A-D, Experimental design: a *Myf5^{Cre};Rosa26^{YFP}* E11.5 embryo is shown under bright light and a fluorescence microscope (**A,A'**). Dotted lines indicate the dissected regions of the pharyngeal arches (**B,B'**) and inter-limb somites (**C,C'**). YFP^{+} cells from these two tissues were isolated by FACS (indicated as R1 in **D**), and used for RNA transcriptome analysis (**E)**. A comparison of gene expression profiles from head (PM, blue) and trunk (somites, magenta) muscle progenitors. The fold change corresponds to the difference in signal intensities **(E).** *In situ* hybridization for *Lhx2* at E8.75 (**F**), E9.5 (**G**), E10 (**H**) and E11 (**I**) embryonic stages matches the microarray data. **J-L**, Transverse sections of control E9.5 embryos, representing the area depicted in (**G**), co-stained with Lhx2 and either AP2 (**J**) or Isl1 (**K-L**). Dotted lines in (**L)** indicate the continuum of PM between the pharyngeal arches and the heart. Black arrowheads indicate *Lhx2* expression in the PM (**F-I**), whereas white arrowheads indicate lack of expression in the inter-limb somites (**G**). 1st/2nd/3rd – first/second/third pharyngeal arches; OFT – out flow tract. Scale bars: 300 μm. Error bars indicate standard error.

Figure 2: Genetic interactions between members of the PM network

A-F', Whole-mount *in situ* hybridization for the indicated genes (left) in E9.5 embryos with the indicated genotypes (black rectangles). Arrows/Arrowheads mark the PM: white arrows, unchanged expression; black arrowheads, down-regulated genes; white arrowheads, upregulated genes. **G**, A ChIP experiment using pharyngeal arch tissues at E9.5 with Tbx1, Pitx2 and Tcf21

antibodies. **H**, A ChIP-seq experiment using Pitx2 antibody on *Pitx2*$^{+/+}$ and *Pitx*$^{-/-}$ pharyngeal arches, reveals specific interactions with *Tcf21*, *Tbx1* and *Lhx2* regulatory regions. **I**, A model summarizing direct (blue) and indirect (grey) genetic interactions in the PM regulatory network. TSS - transcription start site (or proximal promoter); MAE - mandibular arch enhancer. Asterisks point to the indicated TF binding site. Number of embryos in each experiment was ≥3.

Figure 3: Lhx2 is required for specification of pharyngeal muscle progenitors

A-C, Transverse sections of control (**A**) and *Lhx2* mutant (**B**) E11.5 embryos, showing the core of the 1st pharyngeal arch, as indicated in **C**. Dotted lines in A and B represent the magnified areas in D-K. **D**-**F**, Co-immunofluorescence of Pax7 and MyoD in controls (**D**) and *Lhx2* mutants (**E**), and quantification of the results (**F)**. **G-I**, Co-immunofluorescence of myogenic (Pax7 and MyoD) vs. pre-myogenic (Isl1) in controls (**G**) and *Lhx2* mutants (**H**) and quantification of the results (**I)**. **J-L**, Co-immunofluorescence of myogenic (Pax7-MyoD) and phosphorylated histone H3 (P-H3), which labels mitotic cells in controls (**J**) and *Lhx2* mutants (**K**). The percentage of proliferating myoblasts is quantified (**L)**. Quantifications were performed on ≥6 sections from at least two different embryos, as shown in **A–L**. Error bars indicate standard deviation. Antibodies used and DAPI are written in individual panels, in the color corresponding to the fluorescent staining. **M-N**, *Myf5* expression (X-Gal staining) in *Lhx2* control (**M**) and mutants (**N**) E11.5 embryos, which are also heterozygous for the *Myf5*^{nLacZ} reporter. Insets in M-N show the area depicted by the dotted line in **M**. **O-P**, *Myf5* expression (X-Gal) in *Lhx2* control (**O**) and mutant (**P**) E14.5 embryos, which are also heterozygous for the *Myf5*^{nLacZ} reporter. Arrowheads indicate change in muscle patterning. eom-extraocular muscles, 1st/2nd – first/second pharyngeal arch muscle progenitors, fl – forelimb, som – somites.

Figure 4: Epistatic genetic relationships regulating pharyngeal muscle development

A-J, Transverse craniofacial sections of E14.5 mouse embryos stained with MyHC for single (**B-D**) and double (**E-J**) mutants for the indicated genotypes (n ≥4). Dotted line outlines the cleft palate seen in all three single mutants (**B-D**). **J**, A model summarizing the genetic interactions described above. Dotted arrows indicate parallel regulatory interactions affecting head myogenesis, empty

arrowheads indicate novel interactions. Skeletal muscle groups are marked in white arrowheads, and their absence in black arrowheads. eom- extraocular muscles, $1^{st}/2^{nd}$ – first/second pharyngeal arch-derived muscles, tng - tongue.

Figure 5: *Lhx2* and *Tcf21* mutant embryos display specific DGS-like cardiac defects

A-E, Whole-mount E17.5 controls (**A-B**) and *Lhx2*^{mKO} mutants (**D-E**), both displaying normally shaped aortic arches (**B, D** respectively). Note severe anemia in the mutant (**D**) embryo, as compared to control (**A**). A scheme illustrating the normal configuration of the aortic arch (**C**). **F-G**, Hematoxylin and Eosin (H&E) staining of heart paraffin sections in control hearts. **F-M**, *Lhx2*^{mKO} mutants display a simple ventricular septal defect (VSD) (**H-I,** arrow), schematically illustrated (**H**); tetralogy of Fallot (TOF), characterized by both VSD and overriding aorta (**J-K,** arrows); Double outlet right ventricle (DORV, **L-M**). **N-S**, E17.5 *Tcf21* mutant embryos display TOF, VSD, and overriding aorta (**O**) as compared to a control heart (**N**). In addition E17.5 *Tcf21* mutant embryos have pulmonic stenosis, shown by vascular casting (**Q**) and H&E staining (**S**) compared to controls (**P** and **R** respectively). rs – Right subclavian artery; ls – Left subclavian artery; rc – Right common carotid artery; lc – Left common carotid artery; aa – Aortic arch; a – Aorta; p – Pulmonary artery; lv- Left ventricle; la- Left atrium; rv- Right ventricle; ra- Right atrium. The left side of the mouse is displayed on the right side of the picture, in all panels.

Figure 6: PM progenitors form a regulatory network that coordinates early cardiogenesis and craniofacial myogenesis

A. A summary of the genetic interactions of the PM transcriptional network and its impact on cardiogenesis and myogenesis. **B**. A proposed model for a domain specific subdivision of DGS-like anomalies in mouse models into rostral (heart and craniofacial) and caudal (arch artery) phenotypes. The model is based on the progressive alignment of the pharyngeal arches with the heart tube during its looping stages (50). The corresponding mouse knockout phenotypes are shown along these two domains.

Primers for Fig. 5A

ChIP-qPCR

Msc_prom	F	GGCCTAAGTCTTTGCTTTGC	R	TCCGGATCCAAAAGTACAGC
Tcf21_prom_F1	F	AAAGGGGCCTTAGGAGATGA	R	CGAGGAATTTGGTGGACACT
Pitx2ab_prom	F	TCCTTGTCCCTTTCCTACCA	R	GGACCACTAGGGCTGAGAAG
Pitx2c_prom	F	TCTCCTCTCCCCCACCTTAT	R	AGGGATGGTTCTGTCTGCAC
Tbx1_prom	F	CGGAAGGGAAGACATGAAAA	R	ACGCTCCCCAAGTTCTTCTT
Myf5 -40	F	CACCCAAGGCCCATTACCG	R	GTTGTCCTCGGGCCAATACTG

from Zacharias et al. 2010 (http://www.ncbi.nlm.nih.gov/pubmed/21035439)

Myf5 pro	F	AATGTCTTGCTACCGTGCTG	R	GGTCCCTTTGACGCTAATGA
Myf5 -10 kb	F	TCCTTCTCCCACTCTTTCTGA	R	GACATGGCAACTGTGGAATG

Primers for Fig. 5B

ChIP-qPCR

Tbx1	F	TTATGCACCTGCCCAAGACT	R	GGCTGTCAAGAGGTCGTTTC
Tcf21	F	CAGCTCATGTAGGCATCTGG	R	CCGAGGATAAAGCAGGAGTG
Lhx2a	F	TGGCTTTGGTCTCAGAATCC	R	TCCTTTCTGCGGGTCTCTAA
Lhx2b	F	GGCCACATGGCTTTCCCCCAAT	R	TCTTCCACCCCCTCCACACCTT
Lhx2c	F	TGGGTGGACATGCCCTTTCACCT	R	AGAGCCTCAAACCTCACTGTGGC

qPCR

Lhx2	F	CCAGCTTCGGACAATGAAGT	R	TTTCCTGCCGTAAAAGGTTG
Tbx1	F	GCTGTGGGACGAGTTCAATC	R	ACGTGGGGAACATTCGTCT
Tcf21	F	GGCTGGCGTCCAGCTACATCG	R	TGCCGGCCACCATAAAGGGC
Pitx2	F	TGGACCAACCTTACGGAAGC	R	GACAGAGACGTTGACGTGAGG

	E17			E14.5				
	WT	***Lhx2^{mKO}***	***Tcf21$^{-/-}$***	***Lhx2$^{-/-}$***	***Tbx1$^{+/-}$***	***Tbx$^{+/-}$Lhx2$^{+/-}$***	***Tbx1$^{-/-}$***	***Tbx1$^{-/-}$Lhx2$^{-/-}$***
Craniofacial anomalies	0%	0%	100%	100%				
Cleft palate	0%	0%	100%	100%				
Cardiovascular defects	**0%**	**50%**	**30%**	**N/A**				
Tetralogy of Fallot	0%	30% (4/13)	30% (3/11)	N/A				
Persistent truncus arteriosus (PTA)	-	-	-	N/A				
Transposition of the great arteries	-	0%	0%	N/A				
Ventricular septal defects	-	7% (1/13)	0%	N/A	**0%**	**20% (2/10)**	**100% (5/5)**	**100% (4/4)**
Double outlet Right Ventricle	-	15% (2/13)		N/A				
Aourtic arch anomalies	**0%**	**0%**	**0%**	**0%**				
Total	**n=10**	**n=13**	**n=11**	**n=10**	**n=11**	**n=10**	**n=5**	**n=4**

Supplementary experimental procedures:

FACS isolation and microarray screen

Cells were dispersed using a mixture of 0.1% Trypsin and 0.1% Collagenase D (Roche) diluted in F12 (GIBCO). FACS Aria (BD Bioscience) was used to isolate YFP^+ cells. RNA was purified using QIAzol Lysis Reagent (QIAGEN). Due to the small tissue samples, mRNA was amplified (Ambion, Message-Amp kit). Hybridization and detection of the mRNAs were performed on Affymetrix GeneChip mouse expression arrays.

X-Gal staining, histology, immunohistochemistry and in situ hybridization

Antibodies used in the study were as follows: Pax7, MyHC, Pecam1, AP2 and Isl1 (29, 60) and mouse monoclonal antibody (Developmental Studies Hybridoma Bank; 1:5-1:10); MyoD, mouse monoclonal (Santa Cruz; 1:200); Lhx2, Rabbit polyclonal (Santa Cruz; 1:100); phospho-histone H3, mouse monoclonal (Cell Signaling; 1:200). Secondary antibodies used were Cy2-, Cy3-, or Cy5-conjugated anti-mouse or anti-rabbit IgG; Cy3-conjugated anti-mouse IgG1; and Cy5-conjugated anti-mouse IgG2b (Jackson ImmunoResearch, 1:200). Images were obtained with a Nikon 90i florescent microscope with the Image Pro Plus program (Media Cybernetics, Inc.). Images were assembled using Photoshop CS software (Adobe), PTGui stitching software (http://www.ptgui.com) and Canvas (ACD Systems). Percentages given in the text were based on the analysis of ≥6 sections from at least two embryos.

ChIP assay:

The pharyngeal arch tissue was dissected from E9.5 mice, cross-linked with 1% formaldehyde and followed by the addition of glycine to quench formaldehyde. Tissue was washed with ice-cold PBS and lysed in lysis buffer containing a protease inhibitor mixture (Roche). Lysates were sonicated to yield sheared DNA amplicons averaging less than 500 bp. Pre-clearing was

performed with salmon sperm DNA, IgGs from the same origin as the primary antibody, and 45 µl of either protein A or G-Sepharose. Samples were incubated with the following antibodies: goat anti-Pitx2 (C-16, Santa Cruz Biotechnology) overnight at 4 °C followed by the addition of protein A or G-Sepharose for 1 h at 4°C. After several washes, the DNA was eluted from the sepharose beads following incubation overnight at 65°C with RNase A and proteinase K treatment for 2 h at 45°C. DNA was purified with QIAquick columns (Qiagen). PCR analysis using SYBR Green was done to evaluate the relative abundance of sequences in input and IP material. Primers used are listed in supplemental Table 2. Additional ChIP antibodies were Tbx1 (34-9800, Invitrogen); Pitx2 (C16 -sc8748 and H80 - sc33147, Santa Cruz); Tcf21 (ab32981, Abcam, and sc15006, Santa Cruz) and IgG control (ab37355, Abcam). All antibodies we used at 5ug per ChIP experiment.

Vascular Casting

Pregnant mice at E17.5 were anaesthetized by light Isoflurane and one horn of the uterus was surgically exposed. Viable embryos from the uterus were removed and kept in ice-cold PBS. The umbilical artery was exposed by opening the yolk sac and injected with a mixture of PBS and Red Baston's No. 17 Casting Solution for 3-4 min. Embryonic tissues were digested by incubation in 20% KCl for 24-48 hours at room temperature. Casts were examined and photographed on a dissecting microscope.

Figure S1: A screen for PM-enriched regulators

A-B, An example of a single FACS isolation procedure, using cells from either inter-limb somites (**A**) or pharyngeal arches (**B**). Whole mount *in situ* hybridization of E9.5 embryos using *Cyp1b1* (**C**), *Rxrg* (**D**), *Lmo2* (**E**) and *Edn1* (**F**) riboprobes.

Figure S2: Lhx2 is not expressed in PM endothelial cells

A, Whole-mount *in situ* hybridization for Lhx2 at E9.5. B, Lhx2 (green) and Pecam1 (red) staining of of the area marked in (A). 1^{st}, 2^{nd} and 3^{rd} denote the relevant pharyngeal arch.

Figure S3: PM gene expression patterns by in situ sections

A-E', Whole-mount *in situ* hybridization for the indicated genes (left of each image) of E9.5 embryos with the indicated genotypes (black rectangles). Arrows/Arrowheads mark the PM: white arrows, unchanged expression; black arrowheads, down-regulated genes; white arrowheads, upregulated genes. **A-H,** sections for selected embryos, with the indicated genotypes and *in situ* probes. Arrowheads indicate core of the PM.

Figure S4: evaluation of PM gene expression in *Tcf21, Pitx2 and Lhx2* mutants

A, RT-qPCR for selected PM regulators in *Lhx2*, *Tcf21* and *Pitx2* mutants, heterozygous and controls. **B**, X-gal staining of $Tcf21^{-/-}$ ($Tcf21^{LacZ/LacZ}$) at E9.75 compared to $Tcf21^{+/-}$ controls (left). Co-immunofluorescence (at E9.5) for Tbx1 and Pitx2 (βGal), or X-gal staining (at E12.5), in $Pitx2^{-/-}$ and $Pitx2^{+/-}$ control embryos (right). Significant statistical differences ($p<0.05$) are marked with an asterix. To test whether PM cells were present in *Tcf21* mutants; we analyzed E9.5 control *Tcf21* ($Tcf21^{LacZ/+}$) and null ($Tcf21^{LacZ/LacZ}$) embryos. X-Gal staining in the mesoderm core of control and *Tcf21* mutants was comparable at E9.5. In line with this result, pharyngeal muscles were not significantly affected in E14 *Tcf21* mutants. We used the same methodology

in *Pitx2* control (*Pitx2*$^{LacZ/+}$) and mutant (*Pitx2*$^{LacZ/LacZ}$) pharyngeal arches. The mesodermal core, as shown in sections of the 1st arch stained for Tbx1 and Pitx2 (ßGal) proteins, was reduced in *Pitx2* mutants.

Figure S5: ChIP data

A. ChIP for proximal promoters of PM regulators, using Tbx1, Pitx2 and Tcf21 antibodies. The gene expression shown by RT-qPCR is presented relative to the total input. **B**. Additional Pitx2 binding sites on the Tbx1 promoter. **C**. Three putative Lhx2 binding sites on the *Myf5* MAE. **D**, Western blot and ChIP for *Myf5* MAE, using HA antibody and Lhx2-HA construct in vitro (**D**). **E**. An *in vivo* ChIP experiment using pharyngeal arch tissues at E9.5 with Tbx1, Pitx2 and Tcf21 antibodies suggest a range of direct interactions with the Myf5 MAE.

Figure S6: Comparable apoptosis in the PM of controls and *Lhx2* mutants

A, B, Transverse sections of control (**A**) and *Lhx2* mutant (**B**) E11.5 embryos, showing the core of the PM. Co-immunofluorescence of Pax7-MyoD and activated caspase3 (Casp3) cells in control (**A**) and *Lhx2* mutant (**B**) embryos. **C-E**, *Myf5* expression (X-Gal staining) in *Lhx2* control (**C**), heterozygous (**D**) and homozygote (**E**) E11.5 embryos, which are also heterozygous for the *Myf5*^{nLacZ} reporter. Insets in show the area depicted by the dotted line in **C**. Arrowheads indicate change in muscle patterning. eom- extraocular muscles, 1st/2nd – first/second pharyngeal arch muscle progenitors, fl – forelimb, som – somites.

Figure S7: ISH analysis for Lhx2$^{-/-}$ embryos

Whole mount *in situ* hybridization for in E9.5 embryos (Lhx2$^{-/-}$ and controls) for *Fgf8* (**A-B**) *Bmp4* (**C-D**) *Dlx5* (**E-F**) *Sox10* (**G-H**) *Twist* (**I-J**) and Isl1 (**K-L**). White arrowheads indicate

downregulation of Bmp4 in the eye of Lhx2$^{-/-}$ compared to controls (C-D), or defected neural crest migration in Lhx2$^{-/-}$ compared to controls (G-H).

Figure S8: Heart malformations in Tcf21$^{-/-}$ embryos

A-C, Hematoxylin and Eosin (H&E) staining of heart paraffin sections in control hearts (**A**) and enlarged insets (**B-C**). **D-F**, *Tcf21*$^{-/-}$ mutants display tetralogy of Fallot (TOF), characterized by both VSD and overriding aorta (**E,** arrowheads); as well as detached epicardium and aberrant coronary vessels (**F**, white arrows) compared to the controls (**C**). a – Aorta; p – Pulmonary artery; lv- Left ventricle; la- Left atrium; rv- Right ventricle; ra- Right atrium; endo' – Endocardium; myo' – Myocardium; epi' - Epicardium.

Table 1. Genotypes/phenotypes summary table

A table summarizing craniofacial, cardiovascular and aortic arch defects in *Lhx2*^{mKO}, *Lhx2*^{null}, *Tcf21*^{null} and control E17.5 embryos. Because VSD was evident in all hearts of *Tbx1*$^{-/-}$ (n=5), we could not see differences in *Tbx1*$^{-/-}$*Lhx2*$^{-/-}$ (n=4) double mutants due to the saturation of this phenotype.

Table 2. list of primers

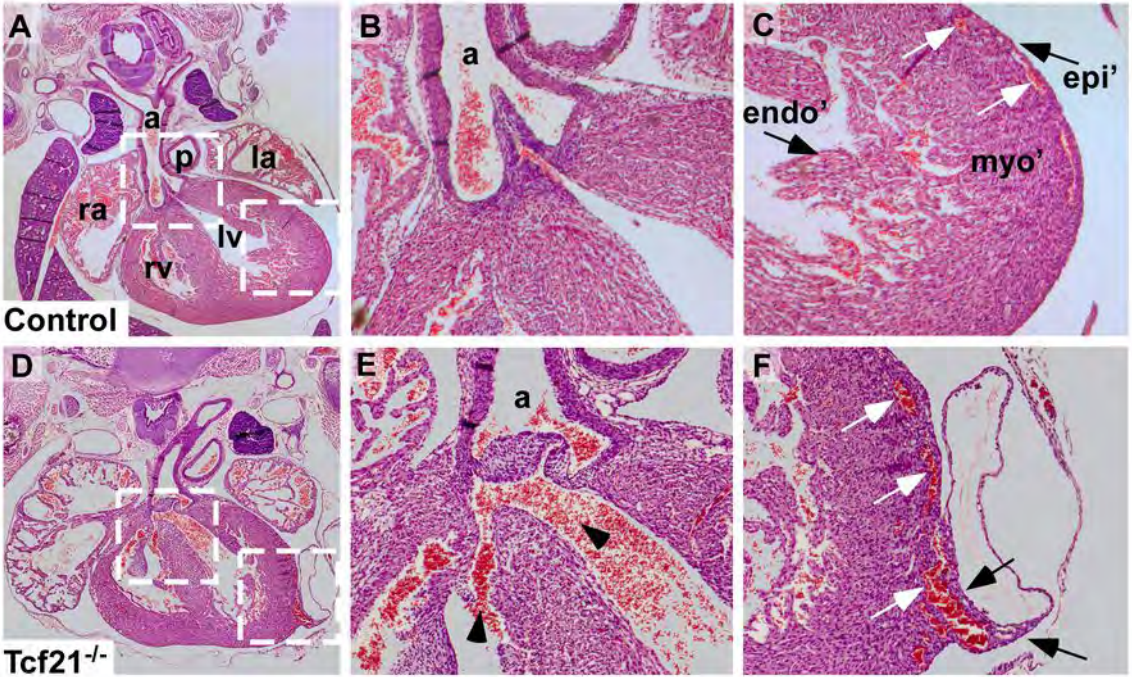
A
a
p
la
ra
lv
rv
Control
B
a
C
epi'
endo'
myo'
D
Tcf21-/-
E
a
F

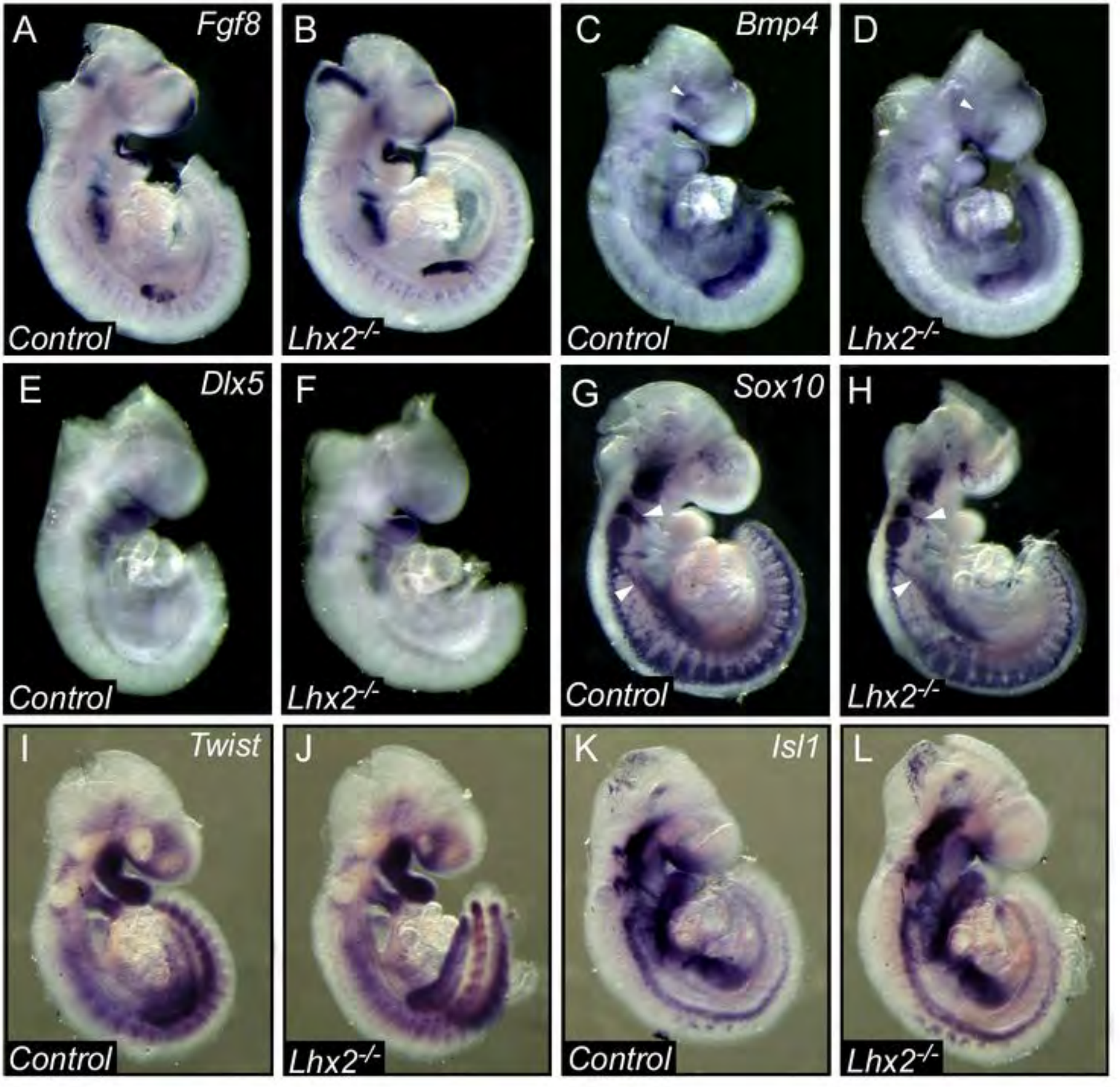
A
Fgf8
Control
B
Lhx2-/-
C
Bmp4
Control
D
Lhx2-/-
E
Dlx5
Control
F
Lhx2-/-
G
Sox10
Control
H
Lhx2-/-
I
Twist
Control
J
Lhx2-/-
K
Isl1
Control
L
Lhx2-/-

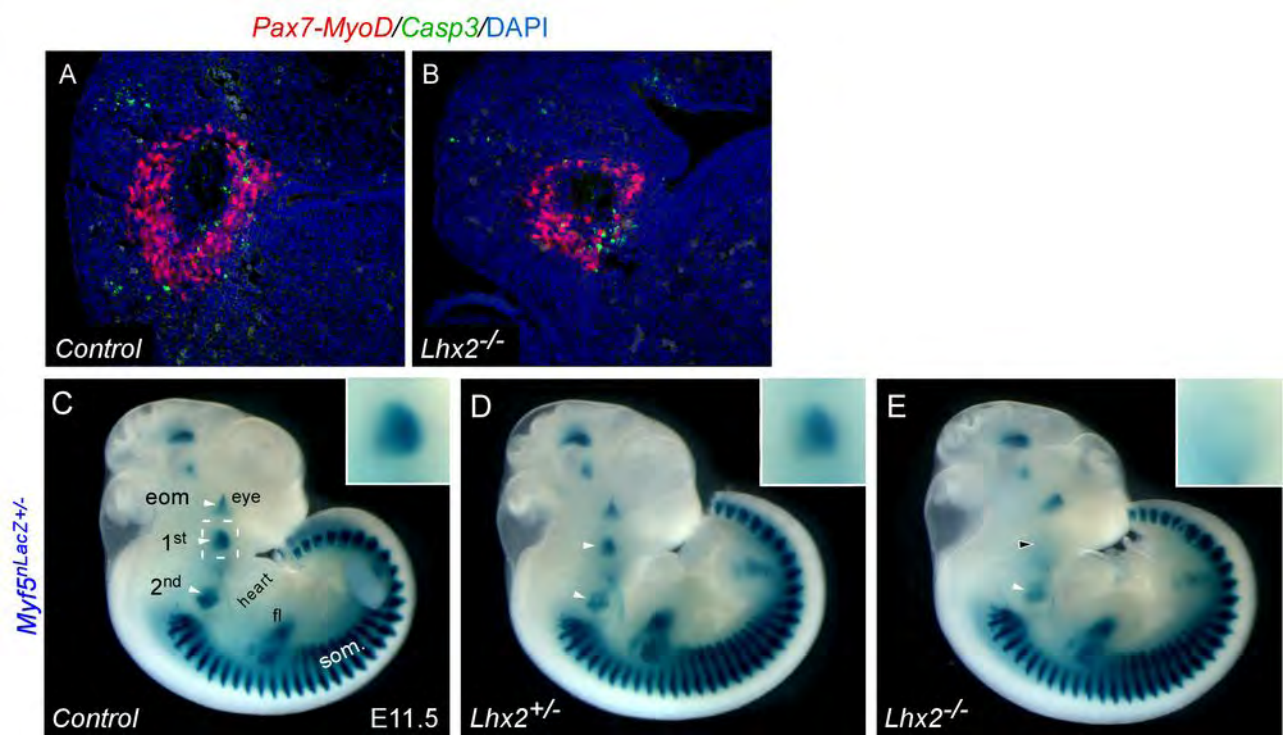
Pax7-MyoD/Casp3/DAPI
A
Control
B
Lhx2-/-
Myf5nLacZ+/-
C
eom
eye
1st
2nd
heart
fl
som.
Control
E11.5
D
Lhx2+/-
E
Lhx2-/-

A. ChIP for proximal promoters using Tbx1, Pitx2 and Tcf21 antibodies:

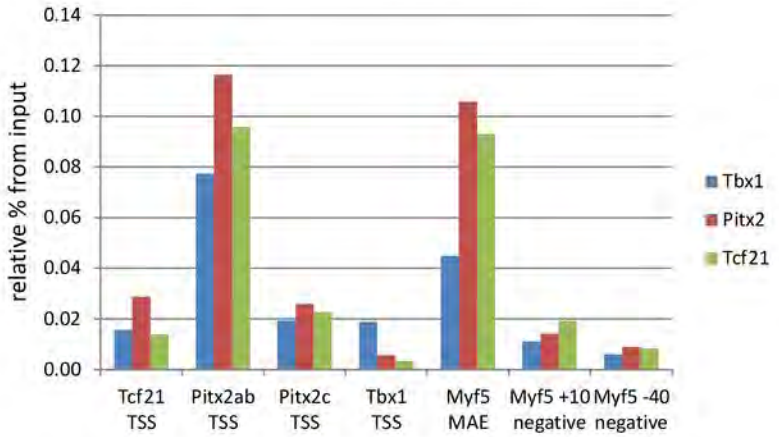

B. Pitx2 binds additional sites on *Tbx1* promoter:

Tbx1 promoter

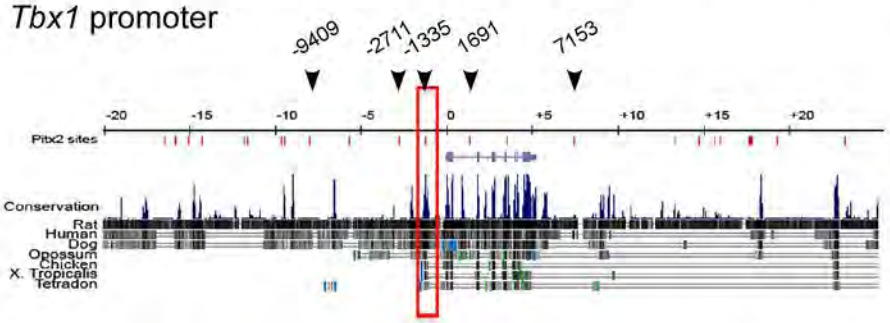

ChIP

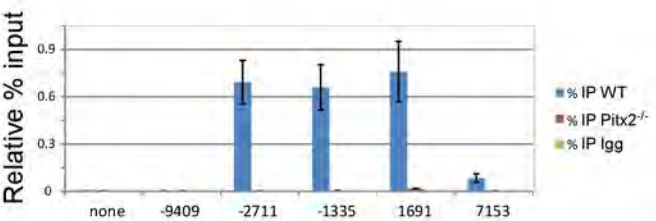

C. Lhx2 binding sites on *Myf5* promoter (Mandibular arch enhancer in Blue):

UCSC Genome Browser on Mouse July 2007(NCBI37/mm9) Assembly

Locations of binding sites:

a) chr10 106,987,527
b) chr10 106,987,604
c) chr10 107,004,375

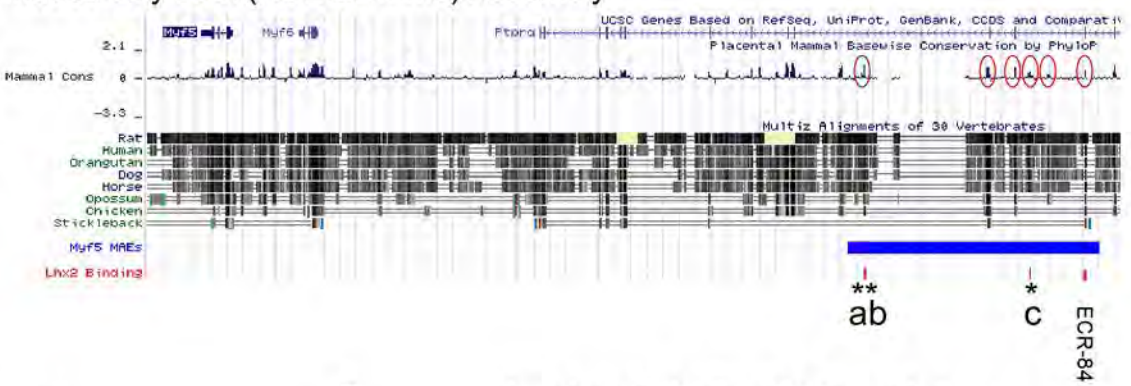

D. Lhx2 and Myogenesis

Construction of Lhx2-HA plasmid HA antibody

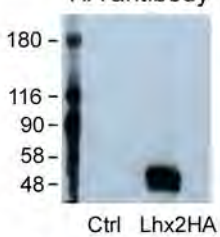

ChIP for Myf5 using Lhx2-HA in C2C12

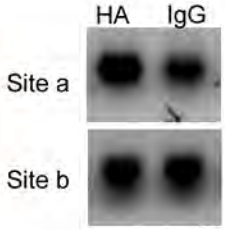

Lhx2 binding to *Myf5* MAE in C2C12

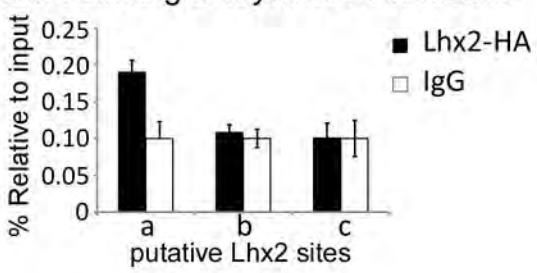

E.

In vivo ChIP for PM regulators

	Myf5 (MAE)	*Myf5* neg. +10kb	*Myf5* neg. -40kb
α-Tbx1	++	-	-
α-Pitx2	+++	-	-
α-Tcf21	+++	-	-

+ weak; ++ moderate; +++ strong binding

A.

qPCR of E9.5 1st-3rd BA

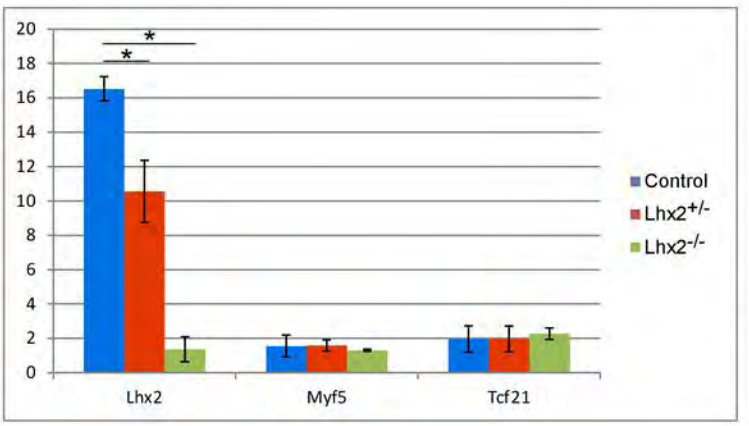

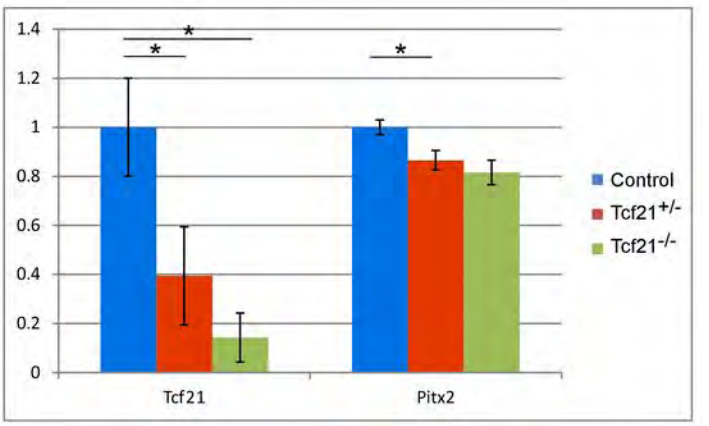

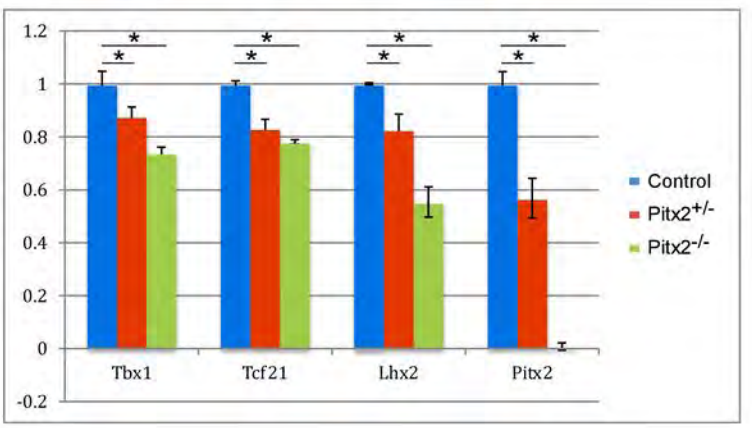

B.

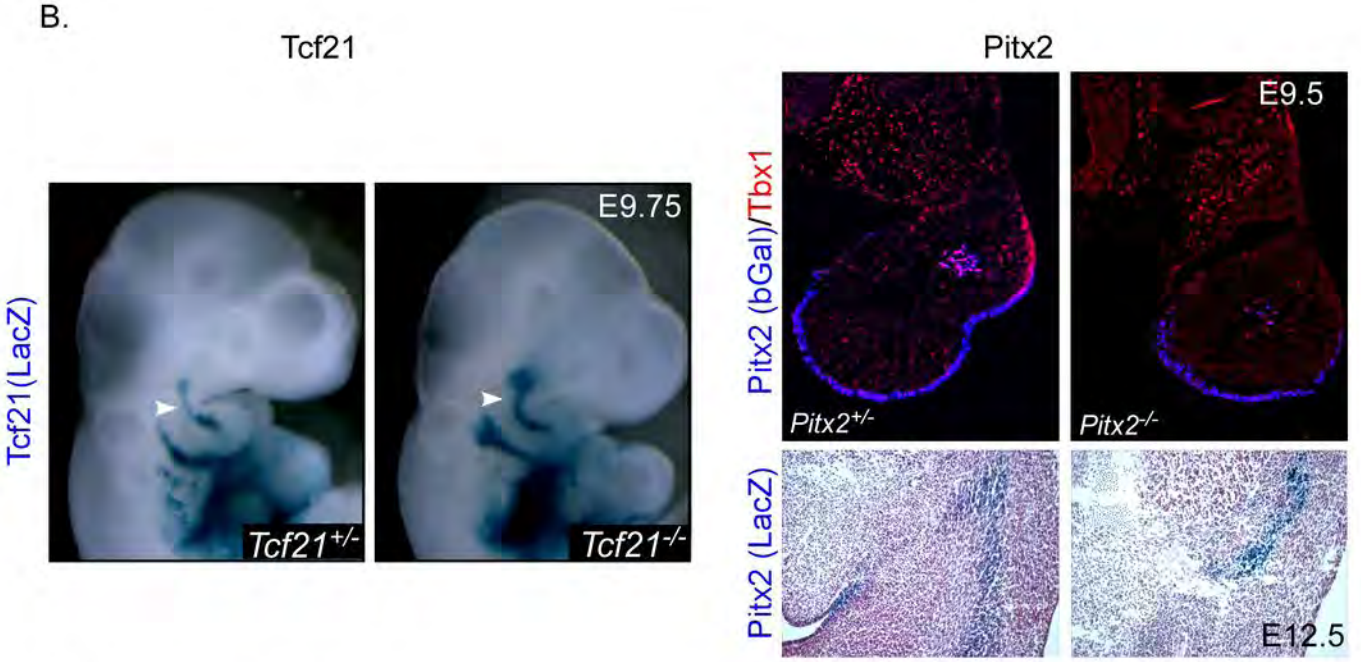

C. Pharyngeal muscles

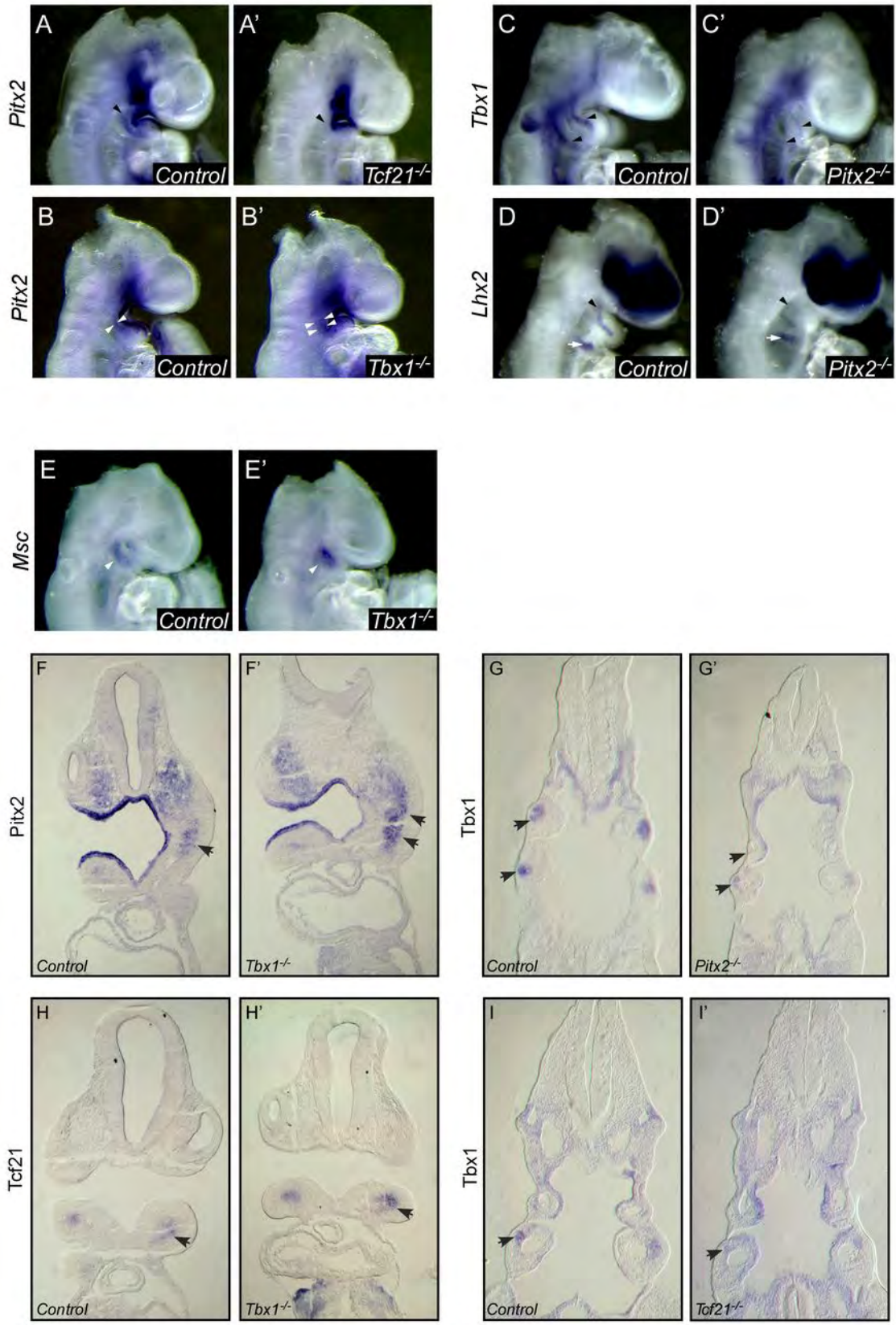
A
A'
Pitx2
Control
Tcf21-/-
B
B'
Pitx2
Control
Tbx1-/-
C
C'
Tbx1
Control
Pitx2-/-
D
D'
Lhx2
Control
Pitx2-/-
E
E'
Msc
Control
Tbx1-/-
F
F'
Pitx2
Control
Tbx1-/-
G
G'
Tbx1
Control
Pitx2-/-
H
H'
Tcf21
Control
Tbx1-/-
I
I'
Tbx1
Control
Tcf21-/-

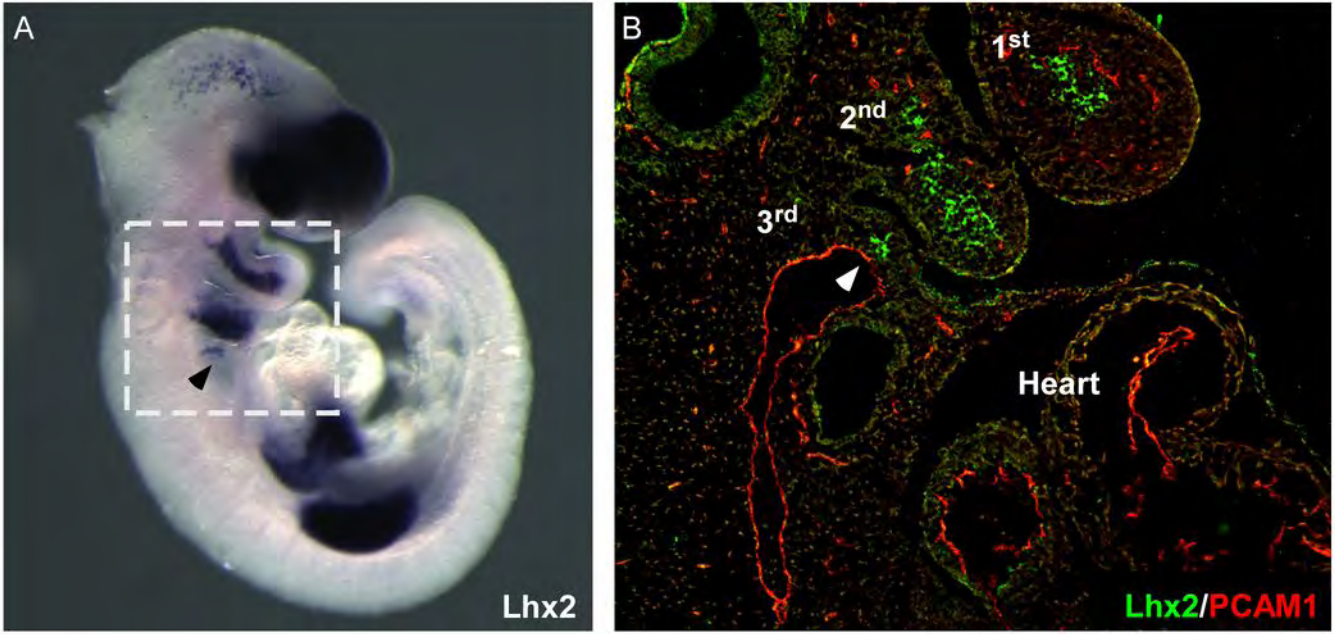
A
Lhx2
B
1st
2nd
3rd
Heart
Lhx2/PCAM1

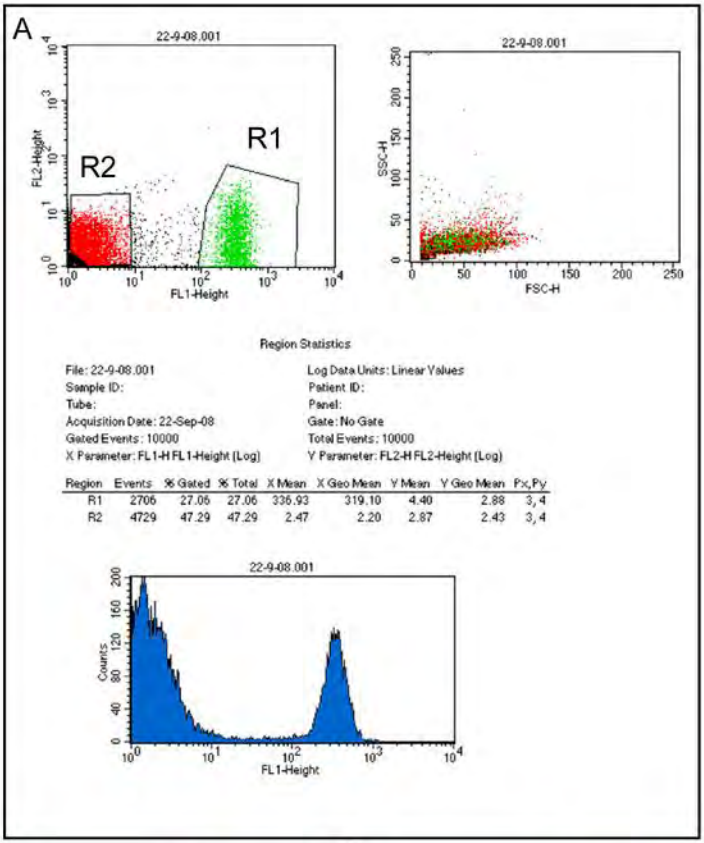
A
22-9-08.001
R2
R1
FL2-Height
FL1-Height
22-9-08.001
SSC-H
FSC-H
Region Statistics
File: 22-9-08.001
Log Data Units: Linear Values
Sample ID:
Patient ID:
Tube:
Panel:
Acquisition Date: 22-Sep-08
Gate: No Gate
Gated Events: 10000
Total Events: 10000
X Parameter: FL1-H FL1-Height (Log)
Y Parameter: FL2-H FL2-Height (Log)
Region Events % Gated % Total X Mean X Geo Mean Y Mean Y Geo Mean Px,Py
R1 2706 27.06 27.06 336.93 319.10 4.40 2.88 3,4
R2 4729 47.29 47.29 2.47 2.20 2.87 2.43 3,4
22-9-08.001
Counts
FL1-Height

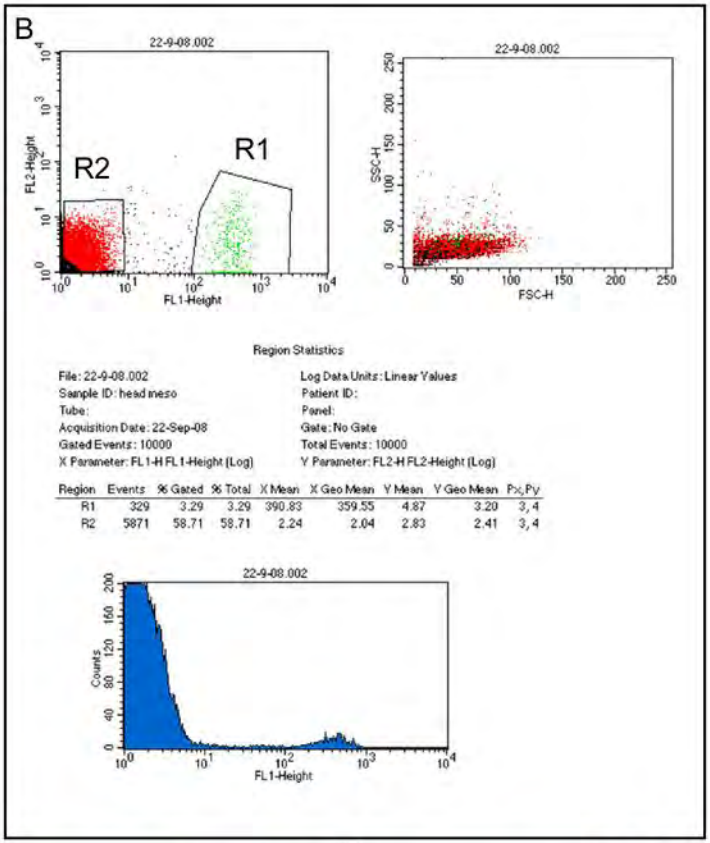
B
22-9-08.002
R2
R1
FL2-Height
FL1-Height
22-9-08.002
SSC-H
FSC-H
Region Statistics
File: 22-9-08.002
Log Data Units: Linear Values
Sample ID: head meso
Patient ID:
Tube:
Panel:
Acquisition Date: 22-Sep-08
Gate: No Gate
Gated Events: 10000
Total Events: 10000
X Parameter: FL1-H FL1-Height (Log)
Y Parameter: FL2-H FL2-Height (Log)
Region Events % Gated % Total X Mean X Geo Mean Y Mean Y Geo Mean Px,Py
R1 329 3.29 3.29 390.83 359.55 4.87 3.20 3,4
R2 5871 58.71 58.71 2.24 2.04 2.83 2.41 3,4
22-9-08.002
Counts
FL1-Height

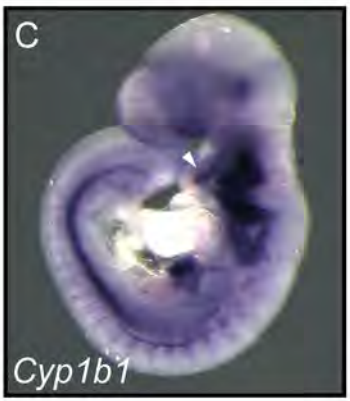
C
Cyp1b1


D
Rxrg


E
Lmo2


F
Edn1

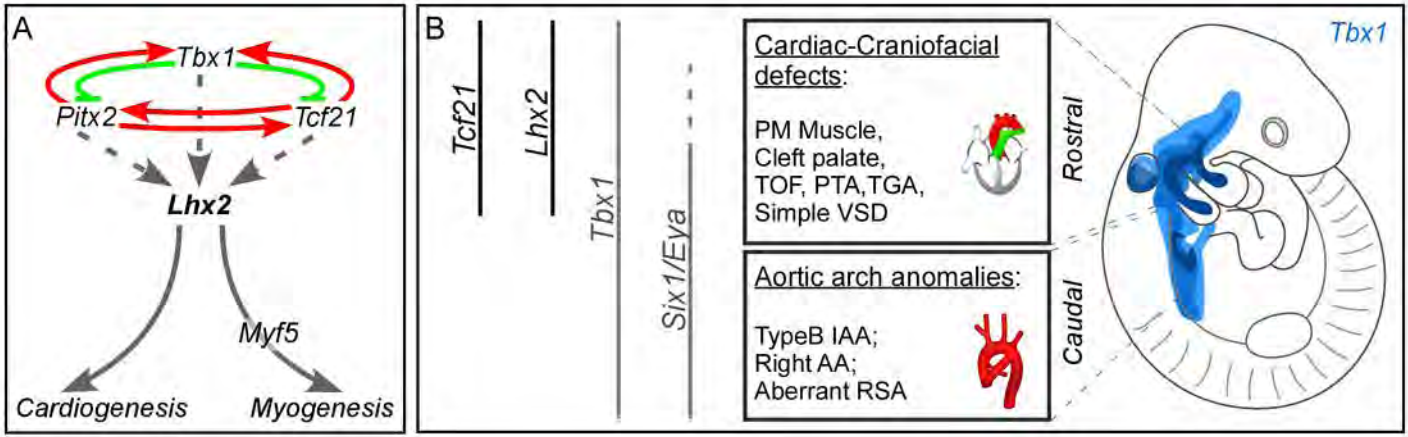
A
Tbx1
Pitx2
Tcf21
Lhx2
Myf5
Cardiogenesis
Myogenesis
B
Tcf21
Lhx2
Tbx1
Six1/Eya
Cardiac-Craniofacial defects:
PM Muscle,
Cleft palate,
TOF, PTA,TGA,
Simple VSD
Aortic arch anomalies:
TypeB IAA;
Right AA;
Aberrant RSA
Rostral
Caudal
Tbx1

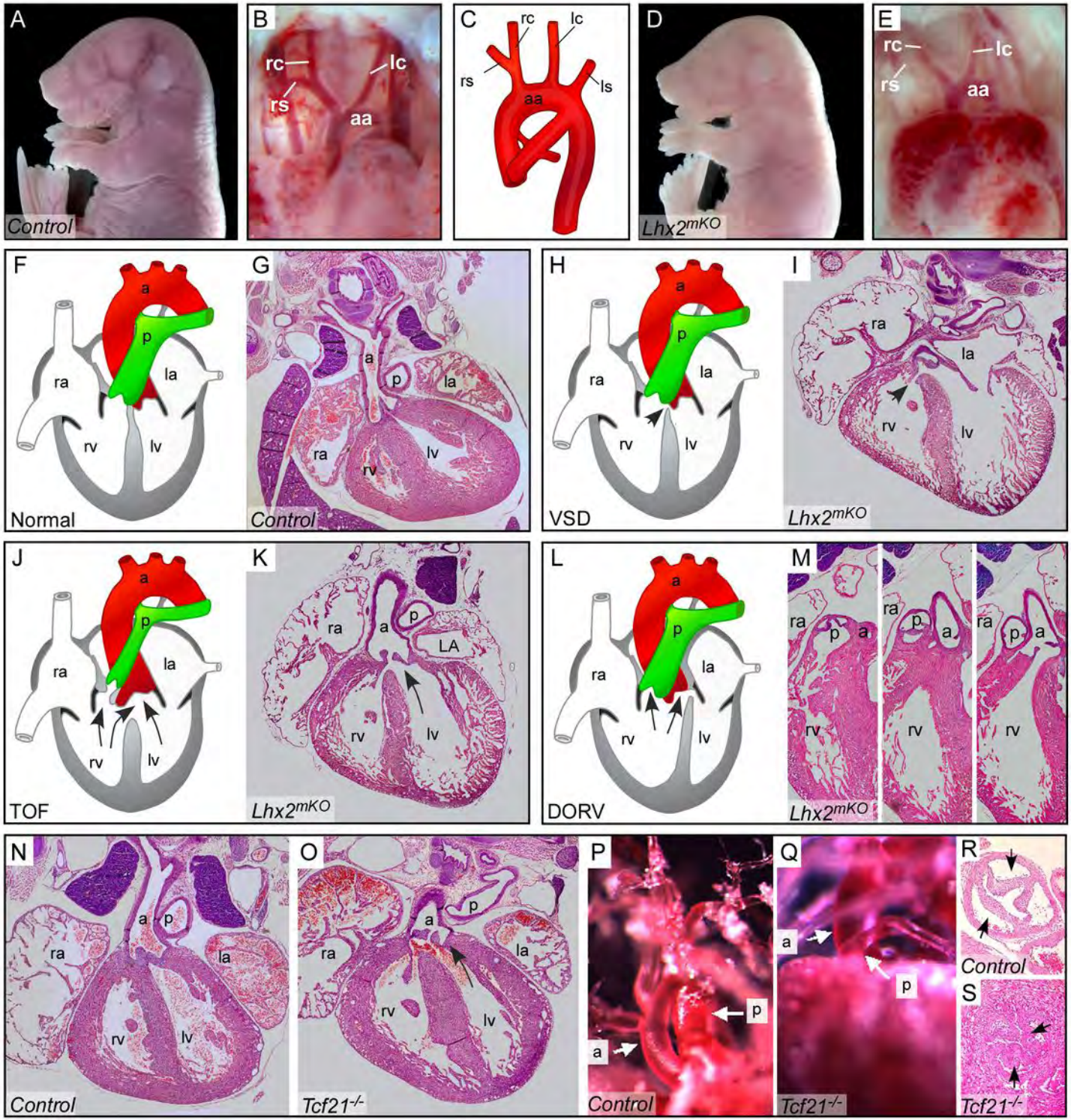
A
Control
B
rc
lc
rs
aa
C
rc
lc
rs
ls
aa
D
Lhx2mKO
E
rc
lc
rs
aa
F
a
p
ra
la
rv
lv
Normal
G
a
p
la
ra
rv
lv
Control
H
a
p
ra
la
rv
lv
VSD
I
ra
la
rv
lv
Lhx2mKO
J
a
p
ra
la
rv
lv
TOF
K
ra
a
p
LA
rv
lv
Lhx2mKO
L
a
p
ra
la
rv
lv
DORV
M
ra
p
a
rv
Lhx2mKO
N
a
p
ra
la
rv
lv
Control
O
a
p
ra
la
rv
lv
Tcf21-/-
P
p
a
Control
Q
a
p
Tcf21-/-
R
Control
S
Tcf21-/-

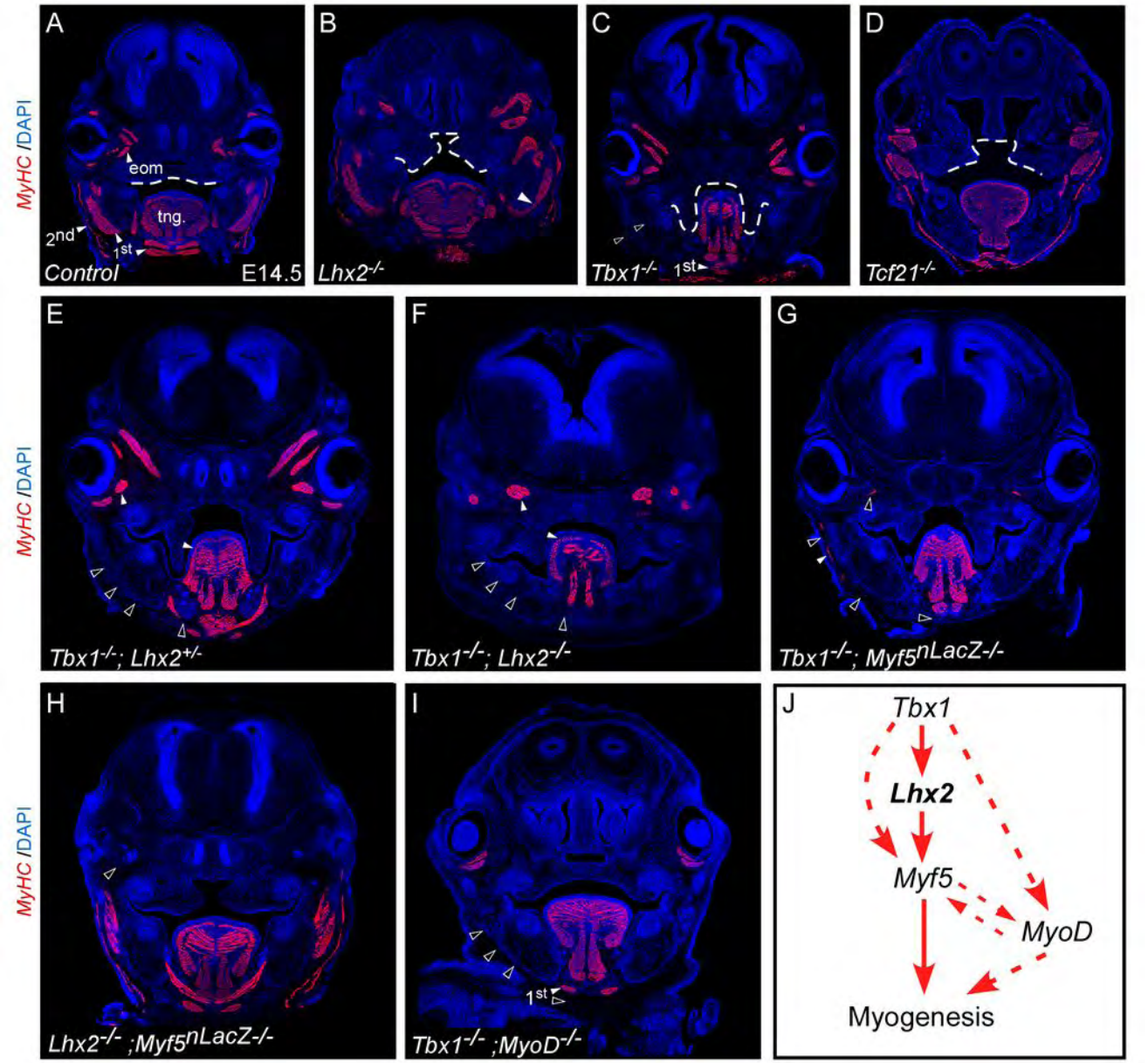
A
B
C
D
MyHC /DAPI
eom
tng.
2nd
1st
Control
E14.5
Lhx2-/-
Tbx1-/-
1st
Tcf21-/-
E
F
G
MyHC /DAPI
Tbx1-/-; Lhx2+/-
Tbx1-/-; Lhx2-/-
Tbx1-/-; Myf5nLacZ-/-
H
I
J
MyHC /DAPI
Lhx2-/- ;Myf5nLacZ-/-
1st
Tbx1-/- ;MyoD-/-
Tbx1
Lhx2
Myf5
MyoD
Myogenesis

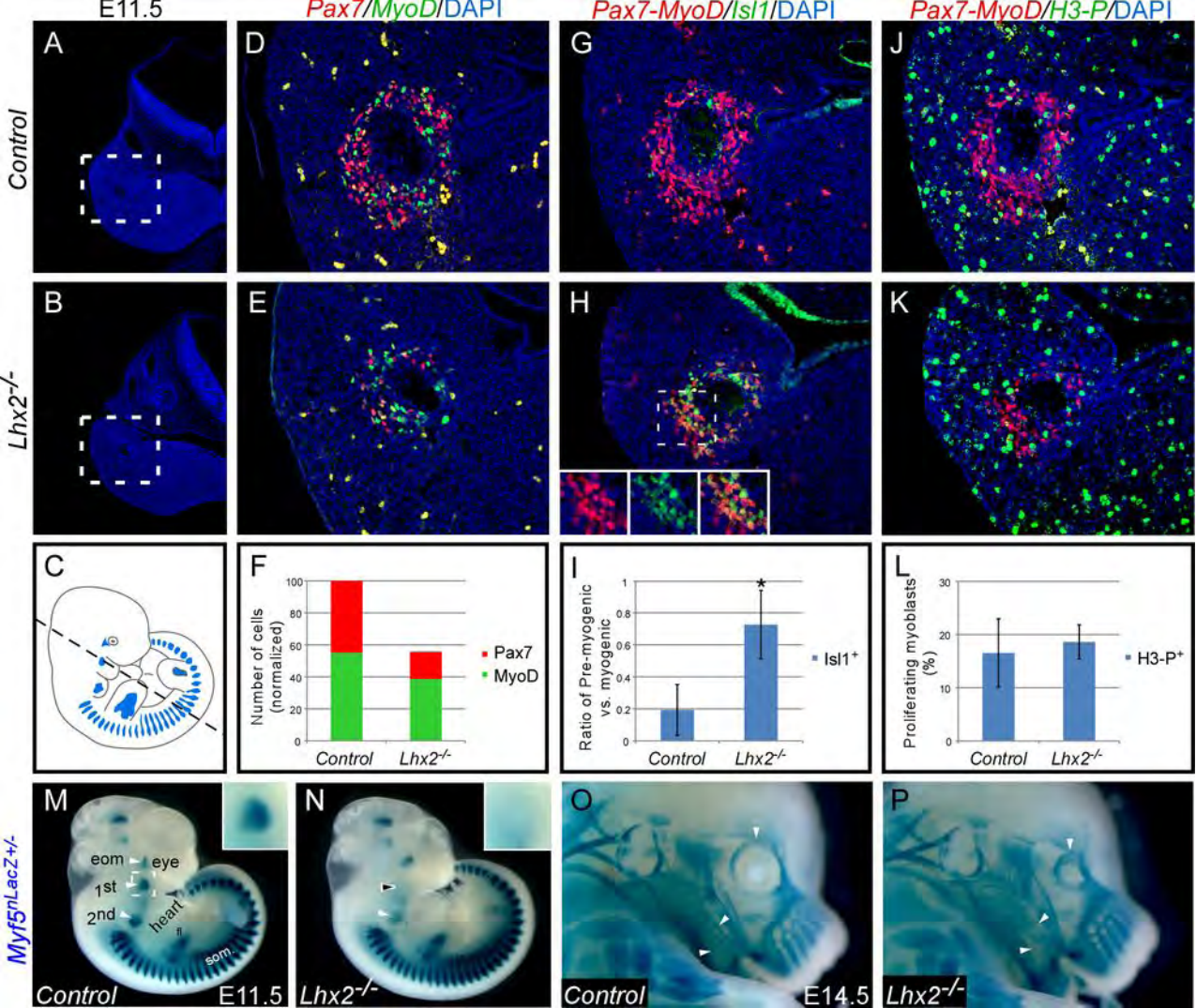
E11.5
Pax7/MyoD/DAPI
Pax7-MyoD/Isl1/DAPI
Pax7-MyoD/H3-P/DAPI
Control
Lhx2-/-
A
B
C
D
E
F
G
H
I
J
K
L
M
N
O
P
Number of cells (normalized)
Pax7
MyoD
Control
Lhx2-/-
Ratio of Pre-myogenic vs. myogenic
Isl1+
Proliferating myoblasts (%)
H3-P+
Myf5nLacZ+/-
eom
eye
1st
2nd
heart
fl
som.
Control
E11.5
Lhx2-/-
Control
E14.5
Lhx2-/-

Gene expression changes in *Lhx2, Tbx1* and *Tcf21* mutants

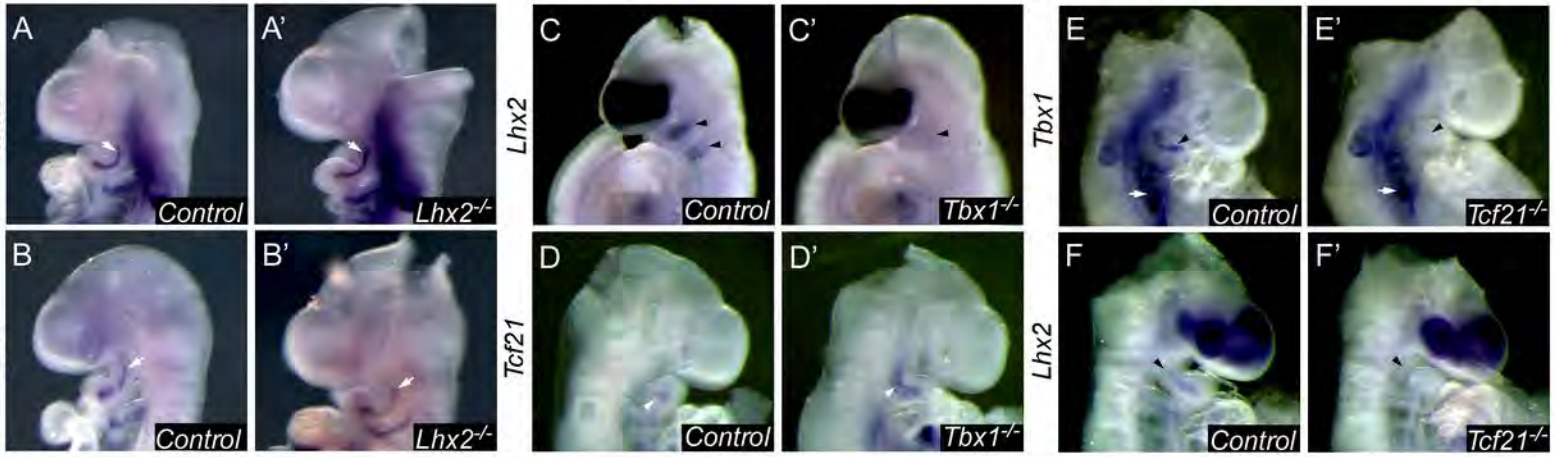

G *In vivo* ChIP for PM regulators

	Tcf21 TSS	*Pitx2ab* TSS	*Pitx2c* TSS	*Tbx1* TSS
α-Tbx1	-	+++	-	+
α-Pitx2	+	+++	+	-
α-Tcf21	-	+++	+	-

+ weak; ++ moderate; +++ strong binding

H *In vivo* ChIP for Pitx2

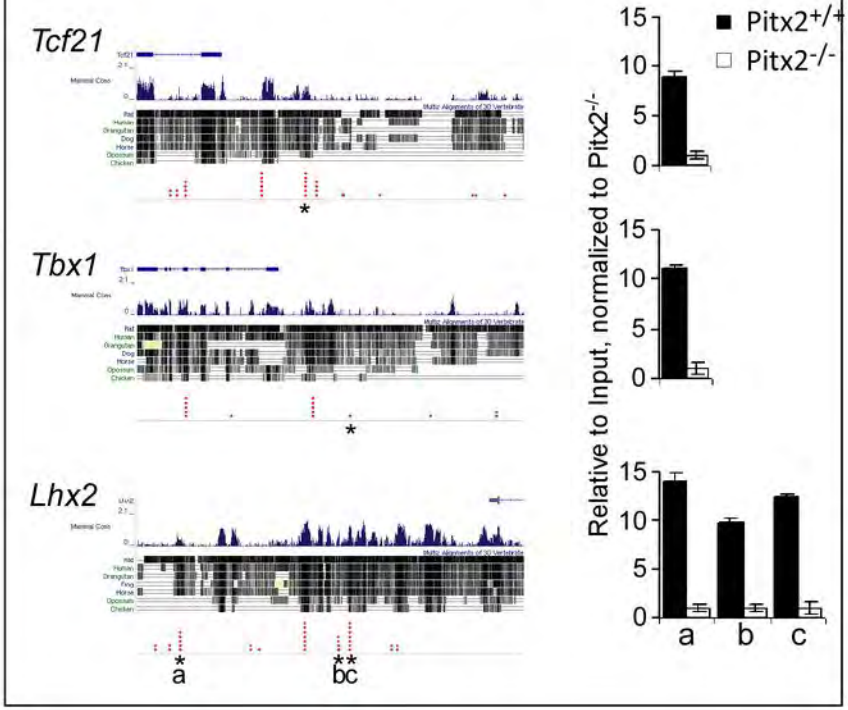

I Interactions between PM regulators

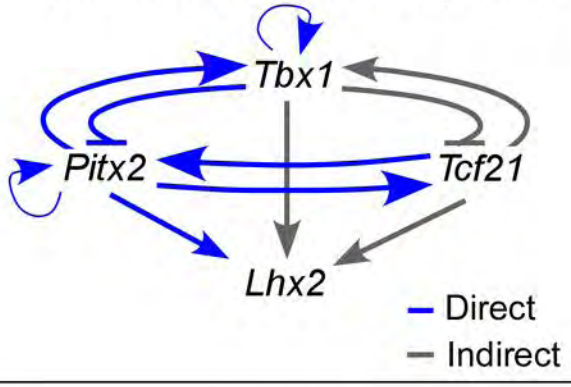

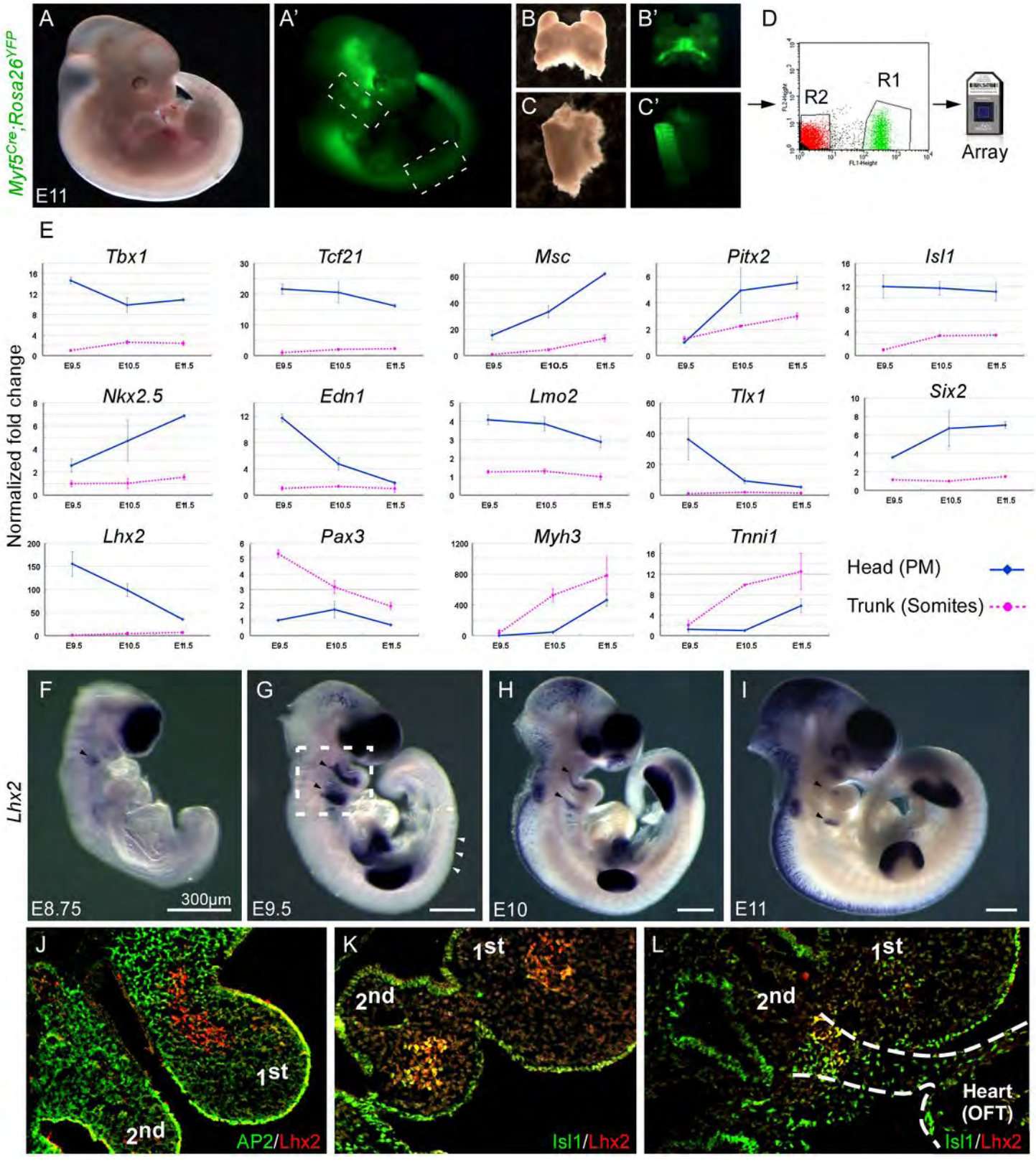
A
A'
B
B'
C
C'
D
R1
R2
Array
E11
Myf5Cre;Rosa26YFP
E
Normalized fold change
Tbx1
Tcf21
Msc
Pitx2
Isl1
Nkx2.5
Edn1
Lmo2
Tlx1
Six2
Lhx2
Pax3
Myh3
Tnni1
E9.5
E10.5
E11.5
Head (PM)
Trunk (Somites)
F
G
H
I
Lhx2
E8.75
300μm
E9.5
E10
E11
J
K
L
1st
2nd
AP2/Lhx2
Isl1/Lhx2
Heart
(OFT)